University of Stavanger

FACULTY OF SCIENCE AND TECHNOLOGY

MASTER'S THESIS

Study programme/specialisation: Petroleum Engineer/ Drilling and Well Technology	Spring semester, 2021 Open
Author: Magnus Håvik Leknes	
Supervisor: Hans Joakim Skadsem	
Title of master's thesis: An Experimental Study of Fluid Displacements and Effects of Inner Pipe Vibration in an Eccentric and Vertical Annulus	
Credits: 30	
Keywords: P&A, Eccentric annulus, Vertical annulus, Reynolds number, Atwood number, Froude number, Pipe movement, Scaling, Through-tubing abandonment, Tubing left in hole, Primary cementing, ELF-rules	Number of pages: 69 + supplemental material/other: 12 Stavanger, 15.07.2021 date/year

An Experimental Study of Fluid Displacements and Effects of Inner Pipe Vibration in an Eccentric and Vertical Annulus

by

Magnus Håvik Leknes

Thesis submitted in fulfillment of
the requirements for the degree of
Master

Faculty of Science and Technology
Department of petroleum Engineering
2021

Abstract

Well abandonment operations can be expensive and time consuming, and thousands of wells will need to be permanently plugged and abandoned off the coast of Norway in the coming years. One potential cost-cutting measure during P&A operations is to leave the majority of the production tubing in the well, which would save significant rig time. However, a big problem with this technique is whether the cement can adequately displace the original fluid, due to tube centralization issues and possibly adverse flow dynamics in the annulus.

In this thesis we present an experimental study of annular displacements and effects of inner pipe vibration. This experimental study serves as a benchmark investigation regarding this vibration-tool when performing through-tubing abandonment. Thus, only Newtonian fluids are considered. The focus is on the effect of eccentricity and the effect of vibration. In an experimental setup, the displacing fluid is pumped into the annulus and displaces the original fluid. The density difference is achieved by adding sugar and salt as weighting agents to the displacing fluid. The fluids are scaled and modelled to simulate real field conditions. In several runs, the eccentricities 0, 0.46, and 0,82 are combined with different vibration intensities (Hz): 0, 2.5, 5, and 10. When the vibration is low and medium, it has an negligible effect on the annulus displacement process when compared to non-vibrating experiments. However, when the vibration intensity is set to 10Hz, we see a significant effect of the displacement process. The high level of vibration enables fluids to flow circumferential from the narrow side to the wide side and vice versa.

Acknowledgement

This thesis is the concluding part of my Master degree in Drilling & Well Technology at the University of Stavanger (UiS). With this I would like to show my gratitude to all involved persons for all help, support and ideas received during the work on this Master Thesis.

Firstly, I would like to use this opportunity to thank my supervisor at UiS/NORCE, Hans Joakim Skadsem, for guidance, support and meetings throughout the project.
Next, I would like to thank Jonas Kristoffer Sunde for all the guidance, ideas, and help regarding the experiments and the setup at NORCE.
Finally, I must express my very deep gratitude to my friends and to family for providing me with unfailing support and continuous encouragement throughout my years of study.

Again, thanks to you all!

Contents

List of Figures

LIST OF FIGURES

List of Tables

Nomenclature

$\dot{\gamma}$	Shear rate (s^{-1})
μ	Viscosity (Pa $\cdot$ s)
∇	Vector differential operator
ρ	Mass density (kg/m^3)
ρ_1	Density of displacing fluid (kg/m^3)
ρ_2	Density of displaced fluid (kg/m^3)
τ	Shear stress (Pa)
τ_y	Yield stress (Pa)
At	Atwood number
D	Diameter (m)
D_H	Hydraulic diameter (m)
Fr	Froude number
g	Gravitational acceleration (m/s^2)
ID	Inner diameter (m)
L	Length (m)
m	Mass (kg)
OD	Outer diameter (m)
P, p	Pressure (Pa)
Q	Volumetric flow rate (m^3/s)
r	Radius (m)
r_i	Inner radius (m)
r_o	Outer radius (m)
Re	Reynolds number
t	Time (s)
t^*	Dimensionless time (=Qt/V)
V	Annulus volume (m^3)
v	Flow velocity (m^2/s)

Chapter 1

Introduction

1.1 Background

A typical oilfield has a lifetime described by figure 1.1. First, the well is produced by pressure declination until it reaches a steady state. It will remain at this plateau before it slowly starts to decrease. As the production shrink toward an economic limit, the wells reaches their last and final stage, the abandonment phase [1]. When the production cost exceeds the income, it is not economically feasible and therefore represents the economic limit [2]. The wells will be closed for production and permanently abandoned. This process is referred to as plug and abandonment (P&A).

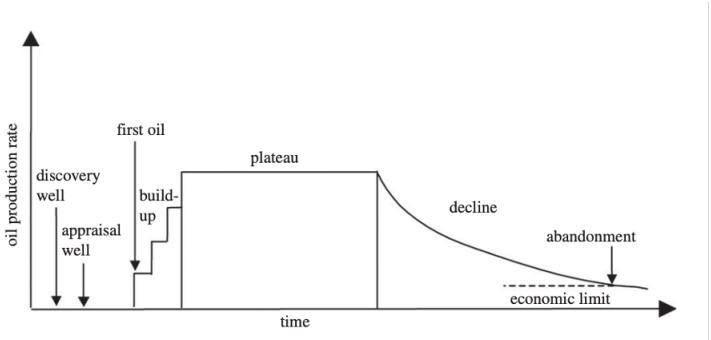

Figure 1.1: *The lifetime of a typical oil field, from discovery to abandonment [3]*

The primary objective of plug and abandonment is to reestablish cap rock functionality in order to permanently maintain well integrity. By installing barriers in the well, we obtain a seal. This shall be installed with a perspective

of eternity. Typically, P&A involve removing the completion equipment and then place a sequence of cement plugs. One option to reduce cost is to leave the majority of the production tubing in the well, which saves valuable rig time. However, a significant challenge with this procedure is whether the cement adequately displaces the original fluid in the annulus. There may be poor cement quality in the annulus as a result of insufficient cement slurry being used in the initial cement work, a lack of tubing centralization causing eccentricity, or unfavorable annular flow dynamics.

A study from 2015 showed that among the 5768 wellbores drilled up to that date, only 3223 had been P&A'ed [4]. This implies that in the future, thousands of wells must be P&A'ed. As much as 40% to 60% of the total cost of a field can be accounted for by P&A [5]. A very cost-effective method is to leave as much tubing in the well as possible. If tubing can be left in hole in a manner that meets long-term abandonment standards, a reduction in cost and duration can be achieved. This should be of interest to everyone, as 78% of the cost falls on the Norwegian taxpayers.

With the increased focus on P&A, multiple companies are expanding within the P&A market by providing new and promising technology. One new technology is a vibration tool that causes the inner pipe to vibrate while annulus cementing combined with through tubing abandonment are performed.

1.2 Statement of problem and objectives

The main purpose of this thesis is to serve as a benchmark study regarding the effect of inner pipe vibration. More precisely, we want to investigate the influence of inner pipe vibration on annular displacement. Additionally,

to evaluate whether vibration has an effect on displacement in wells with a high level of eccentricity. Furthermore, we want to study if the tool prevents slower fluid front velocities on the annulus's narrow side and promotes more uniform fluid front velocities by enabling fluid exchange from the narrow to wide side.
Summarize of objectives:

- Study the effect of vibration on the annular displacement.
- Study if some conditions can obtain a more steady displacement pattern.
- Study if the fluid will propagate equally on the wide and narrow side of the annulus.
- Vary the eccentricity and vibration to see the effects.

1.3 Limitations

This investigation is limited to Newtonian fluids. Laminar flow regimes are being investigated. Furthermore, the experimental configuration is vertical. This study excludes displacement involving immiscible fluids such as oil and water, non-Newtonian fluids, high viscosity fluids, and turbulent flow regimes.

1.4 Structure of Thesis

The remaining part of this thesis will be structured in the following way:

- **Chapter 2** defines the theory needed to better understand the results. It includes cementing technique, eccentricity, fluid rheology, ELF-rules,

pipe movement, scaling and modelling, as well as governing equations and dimensionless numbers.

- **Chapter 3** includes a detailed methodology of the experiments performed, scaling and selection of fluids, and the experimental setup.
- **Chapter 4** presents the results of the experimental work and a discussion of these.
- **Chapter 5** aims to summarize and conclude based on the the objectives presented in section 1.2. Recommendations for further work are also presented.

Chapter 2

Theory

2.1 Primary cementing

During primary cementing, cement is placed in the annulus between the casing and the formations exposed to the wellbore. Primary cementing and annulus cementing are used to provide zonal isolation in oil, gas, and water wells, i.e., separating fluids such as water or gas in one zone from oil in another zone. This requires the establishment of a hydraulic seal between the casing and the cement, as well as between the cement and the formations, while at the same time avoiding the formation of fluid channels in the cement sheath. As a result of this necessity, primary cementing is one of the most critical operations conducted on a well. Without total isolation within the wellbore, the well may never produce to its maximum capacity. After the well reaches the required depth of the section, the drillpipe is withdrawn, and a string of casing or liner with a bigger diameter is run to the bottom of the section, typically leaving a gap of approximately 2 cm in the annulus. The annulus refers to the space between the casing and the formation, the casing and the casing, or the casing and the liner. The drilling mud is still in the wellbore at this stage. This mud must be eliminated and substituted with a cement slurry and/or spacer fluid. To avoid contamination with mud, two plugs isolate the cement as it is squeezed down the casing. A sufficient amount of cement slurry is injected into the casing to completely fill it from

the bottom to the top of the productive zones. Finally, the well is closed for a period of time to let the cement solidify enough before completion activities or drilling to a deeper horizon may commence. The process is shown in figure 2.1. Typically, cement slurry is pumped to higher altitudes to isolate the wellbore from other undesired fluids, to preserve freshwater zones, to preserve the casing from corrosion, and to provide structural support for the casing [6] [7].

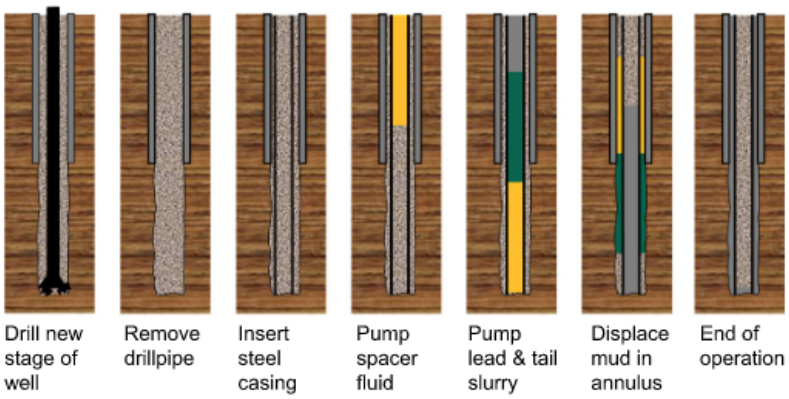

Figure 2.1: *Schematic of the primary cementing process, illustrating the various processes (left to right) involved in cementing a new casing [7]*

2.2 Through-tubing abandonment

Through-tubing abandonment is when well completions are left in the hole and permanent barriers are installed through and around the tubular by pumping cement down the production tubing. The cement is entering the A-annulus by punched tubing or cut tubing at the base just above the production packer. Induced holes followed by cement squeezing. Before starting the through-tubing abandonment, reliable methods and procedures concerning the barrier placement and verification should be established.

2.2 Through-tubing abandonment

The packer depth must be more than 100ft below the abandonment horizon [8]. According to UK Guidelines, if the verification of the barrier position is based on differential pressure alone or other measurements excluding logging, 1000ft MD of cement is recommended in the B-annulus. If it is logged, it is required a minimum of 200ft/100ft good cement depending on if it is a combination barrier or a single permanent barrier (primary and secondary) [9]. According to NORSOK, the minimum requirements for an annular barrier is 30m MD cement verified by bonding logs or 50m MD cement by calculating the displacement [10].

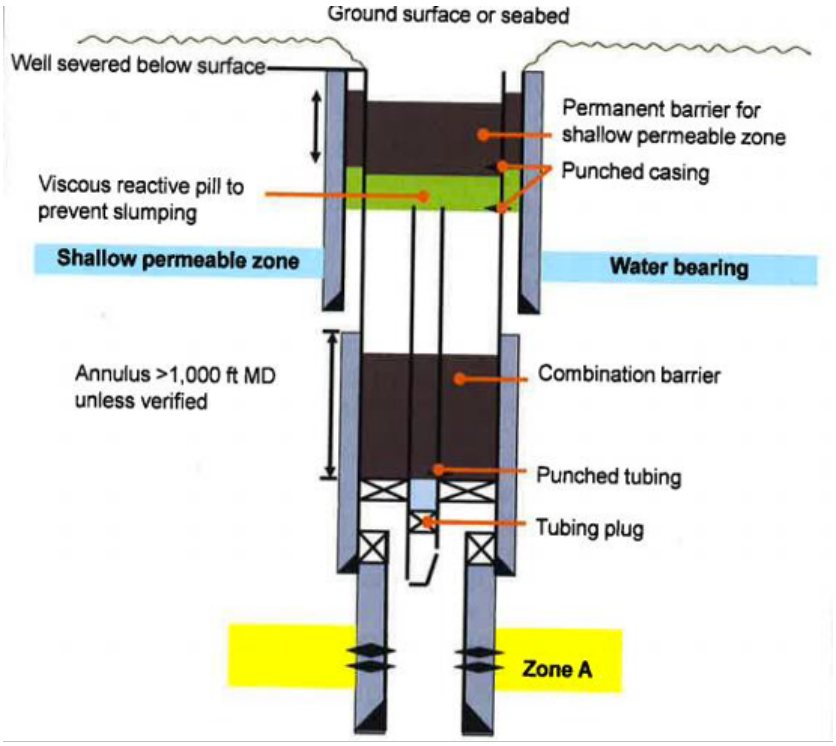

Figure 2.2: *Through-tubing abandonment with combination barrier [11]*

2.3 Wellbore eccentricity

When cementing in the field, the casing is almost never perfectly centered in the wellbore, even when centralization tools are used to minimize eccentricity. In the case of decentralization, the casing is closer to one side than the other. The annular space that is created is often described as eccentric. Eccentricity is defined as the distance between the centers of the two cylinders, divided by the difference in radius:

$$e = \frac{\delta}{r_o - r_i} \tag{2.1}$$

Where δ is the offset between the cylinder axes, r_o is the outer diameter, and r_i is the annulus inner diameter.

This distance between the centers is often characterized by eccentricity, e. This can vary from 0 – 1, where 0 means a perfectly centralized pipe, while the value 1 means that there are contact between casing and wellbore. In vertical wells the use of centralizers are rarely used, so it is reasonable to assume that the eccentricity of vertical wells is determined by the collar dimensions. In near-horizontal wells, a value of e close to 1 can happen, but it is rarely achieved in vertical wells. In the field, it is typically a value in the range of $e \in [0, 0.6]$ [12]. These values can suitably be covered in this thesis. As well as the extreme cases where e is getting closer to 1. Figure 2.3 illustrates different scenarios:

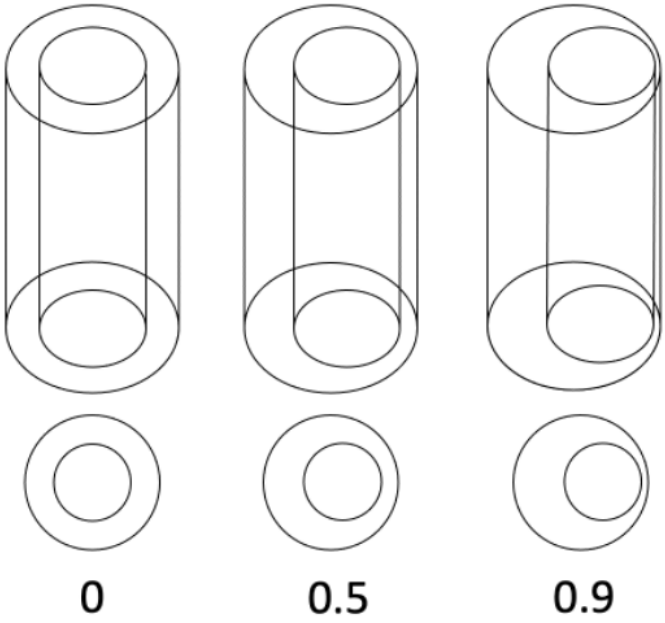

Figure 2.3: *Graphic representation of eccentric annulus*

Displacement of fluids in the annulus is strongly dependent on eccentricity. Therefore this needs to be considered. When the annular space is eccentric, the flow will not be uniform. The displacing fluid will follow the path of least resistance [13]. Hence, it will flow in the wider part of the annulus. This may result in rare scenarios in which the flow regime is laminar on the narrow side and turbulent on the wide side [6]. The fluids in the narrow part can be bypassed or even become static. The critical flow rate is strongly dependent on the value of e. It is essential to achieve this flow rate to ensure sufficient flow in the narrow gap. Figure 2.4 illustrates different scenarios:

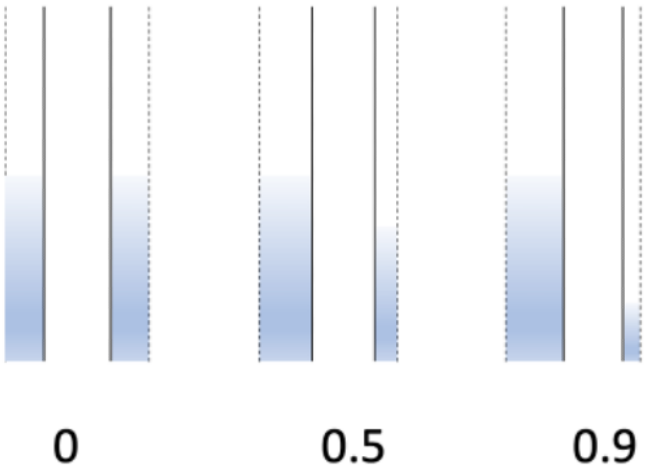

Figure 2.4: *Effect of flow due to eccentricity. Choose wide side*

Another measurement of eccentricity is stand-off, which can be calculated as [14]:

$$Stand - off = \frac{C}{A - B} \tag{2.2}$$

Where A = Wellbore radius, B = Pipe radius, and C = Shortest distance between the pipe and the wellbore wall.

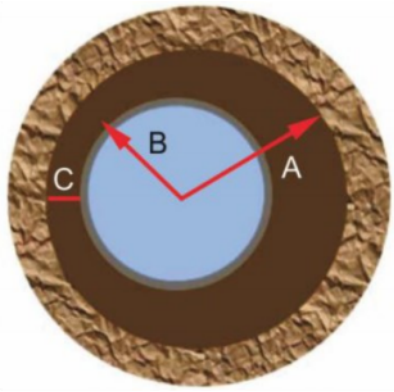

Figure 2.5: *Illustrating A, B and C*

2.4 Displacement efficiency

The displacement efficiency is the most used parameter to describe a fluid's capacity to displace another. This parameter is referred to as the circulation efficiency when the same fluid is utilized to displace itself. A typical displacement-efficiency curve is shown in figure 2.6. Although circulation or displacement efficiency is a straightforward principle, it may occasionally be deceptive, particularly at large eccentricities. Under such conditions, a wide angular channel of bypassed mud in the annulus's narrow section would represent a small percent of the total flow area (Figure 2.6). The displacement is quite effective across the majority of the casing; nonetheless, there is a continuous mud channel remaining. Additionally, a thin layer of mud on the formation and casing walls may stay immobile [6].

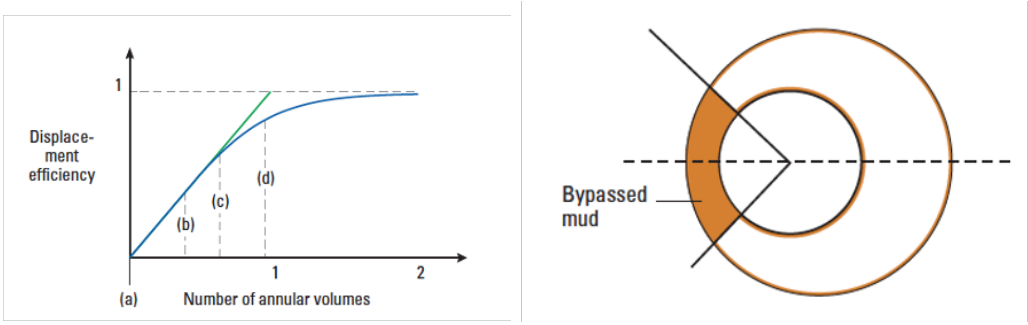

Figure 2.6: *Schematic of a displacement-efficiency curve, with an asymptotic value equal to unity (left), and schematic of mud bypassed in an eccentric annulus (right)* [6]

The displacement efficiency can be calculated as [6]:

$$t^* = t \cdot \frac{q}{V_{ann}} \tag{2.3}$$

Where t^* is the dimensionless time, q is flowrate, and V_{ann} is the volume of the annulus. The dimensionless time is equal to the number of annular

volumes pumped. At time t = 0, the displacing fluid suddenly replaces the displaced fluid at the annulus's entrance. At any moment t > 0, the displacement efficiency is the fraction of annular volume occupied by the displacing fluid. The time at which the displacing fluid appears at the annulus's outlet is referred to as the breakthrough time, t^*_{break}. This is shown in Fig 2.6, point (c).

Density hierarchy is a concept that describes the ordering of fluids with varying densities. Typically, the density of the displacing fluid is larger than that of the displaced fluid during a displacement process. This is done to improve the displacement efficiency since the heavier fluid displaces the lighter fluid. This is performed in a specific order to attain a sufficient displacement efficiency. For instance, in cementing operations, the density hierarchy is as follows:

$$\rho_{mud} < \rho_{spacer} < \rho_{cement} \tag{2.4}$$

2.5 ELF Rules

The casing string is almost always decentralized in the field, even for vertical wells [15]. This eccentricity results in slower flow velocities in the narrow part of the annulus and higher flow velocities in the wide part. The eccentricity will lead to poor displacement on the narrow side of the annulus unless the displaced fluid and the displacing fluid are compensated for by density and/or viscosity differences [16]. To improve the effectiveness of laminar displacements, industry-standard guidelines have been developed. The guidelines have been developed to achieve a steady-state

displacement by validating different hierarchies such as density and viscosity etc. One example of this is ELF- rules. Effective laminar flow guidelines. They are presented below [16][17]:

Rule (1) – The displacing fluid should be at least 10% heavier than displaced fluid.

$$\rho_2 > 1.1\rho_1 \tag{2.5}$$

Rule (2) – The friction pressure gradient exerted by the displacing fluid should be at least 20% larger than that of the displaced fluid.

$$\left(\frac{dP}{dz}\right)_{2,friction} > 1.2\left(\frac{dP}{dz}\right)_{1,friction} \tag{2.6}$$

This implies that the displacing fluid must be more viscous and less mobile than the displaced fluid.

Rule (3) – The pressure gradient on the narrow side of the annulus must exceed the gel strength of the displaced fluid.

$$\left(\frac{dP}{dz}\right)_{2,friction} + (\rho_2 - \rho_1)g\ cos\theta\ >\ \frac{2\tau_{y,1}}{h} \tag{2.7}$$

Where $(^{dP}/_{dz})_2$ is the friction pressure gradient in an equivalent concentric annulus for the displacing fluid. Additionally, $\tau_{y,1}$ represent yield stress of fluid 1, which is the displaced fluid. Some fluids have the ability to behave like gel when exposed to no flow for an extended period of time. The gel strength will start to behave like a fluid again when exposed to a certain yield stress. This is referred to as the yield point.

θ is the inclination from vertical and h can be expressed as $h = (1-e)(r_o-r_i)$. This characterizes the radial gap on the narrow side of an eccentric annulus.

Rule (4) – The flow resistance of the displacing fluid on the wide side of the annulus must be larger than that of the displaced fluid on the narrow side

$$\left(\frac{dP}{dz}\right)^{wide}_{2,friction} + \rho_2 g\ cos\theta\ >\ \left(\frac{dP}{dz}\right)^{narrow}_{1,friction} + \rho_1 g\ cos\theta \tag{2.8}$$

Where $(^{dP}/_{dz})^{narrow}_1$ is the friction pressure gradient in an equivalent concentric annulus where the radius is kept the same as the narrow side of the original. Likewise, $(^{dP}/_{dz})^{wide}_2$ is the friction pressure gradient in an equivalent concentric annulus where the radius is kept the same as the wide side of the original.

The density and viscosity hierarchies are being ensured by ELF rules number one and two, respectively. The denser and more viscous fluid is the displacing fluid, and the lighter and less-viscous fluid is the displaced fluid. These two rules ensure that the displacing fluid is underneath the displaced fluid in a near-vertical annulus. The third ELF rule describes the mobilization of the displaced fluid. The fourth and final rule ensures that the fluid interface is a stable front by validating that the displacing fluid is not flowing faster on the wide side than displaced fluid on the narrow side [16]. When calculating the pressure gradient, the Hagen-Poiseuille equation for Poiseuille flow in an annular section is used [18]:

$$Q = \frac{G_\pi}{8_\mu}\left[R_2^4 - R_1^4 - \frac{\left(R_2^2 - R_1^2\right)^2}{\ln\ {}^{R_2}/_{R_1}}\right] \tag{2.9}$$

To find the pressure gradient, this equation is solved for G.
Where $G = -{}^{dP}/_{dz}$, R_2 is the outer cylinder radii, R_1 is the inner cylinder radii, and μ is the fluid viscosity.

2.5.1 Steady stable displacement

When a flow maintains consistent temperature, velocity and other parameters with respect to time, it is considered to be steady. On the other hand, unsteady flow may have changes in mass, pressure or energy and becomes time-dependent. To ensure a steady displacement, the interface between two fluids must move continuously along the displacement area. This implies that the form of the interface between the two fluids must remain consistent throughout the displacement profile [19]. See fig 2.7. Steady displacement is desirable for cementing operations because it ensures continuous and complete displacement around the whole annulus. A steady displacement helps minimize mixing of the two fluids, as well as it aid to eliminate residual drilling fluid in the annulus [20].

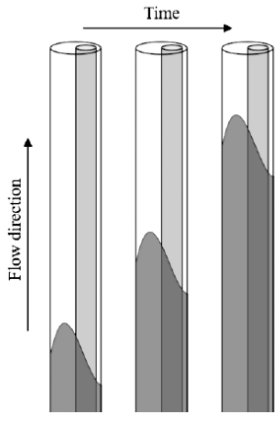

Figure 2.7: *Steady displacement in eccentric annulus [21]*

2.6 Casing movement

Rotation and reciprocation along their axes are the two primary methods of tube movement [6]. The effective volume of drilling fluid moving in the annulus increases when introducing pipe movement. This also aids in breaking the gel strength of immobilized mud or curing cement that otherwise would not be broken by flow rates, fluid rheology, or centralization. The fluid will flow in a circumferential direction when the pipe is rotated and will enable transferring of fluid from the narrow side to the wide side and vice versa. The rotating of the pipe helps to remove the mud which would become trapped on the narrow side of an eccentric annulus without pipe movement.

Reciprocating the pipe causes lateral movement and will change the flow area, encouraging mud displacement. The introduction of a dynamic condition by rotating and reciprocating the casing will enable the constant flow velocity to remove mud easier in both the wide and narrow parts of the annulus [14]. Casing movement—whether reciprocal or rotational — is considered to improve the quality and reliability of primary cement jobs [6]. However, in this thesis it will presented a vibration-tool with heavily lateral movement combined with a small oscillating movement instead of rotational movement. When rotation and reciprocation are not possible during P&A, the vibration tool in this experiment is applicable. The objective of this tool is to enhance the displacement on the narrow side in an eccentric annulus.

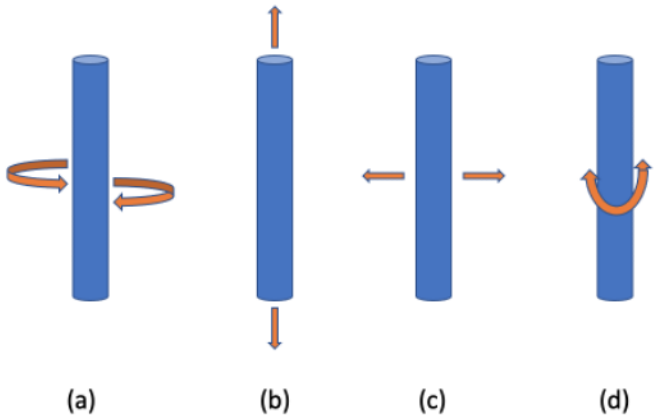

Figure 2.8: *Different pipe movements: (a) Rotational, (b) Reciprocal axial, (c) Lateral, and (d) Oscillation*

2.7 Rheology

To plan, execute, and assess a primary cement job successfully, it is necessary to first understand the rheological properties of the fluids used [6]. The oil and gas business heavily relies on rheological characterization. Cement, drilling fluids, workover fluids, production fluids and completion fluids are all affected by rheology. All substances, whether solids, liquids, or gases, will eventually flow if given adequate time and force. Rheology is the science of how materials flow in response to changes in shear rate, spatial orientation, and time. Pressure, temperature, and the rate and duration of shear all have an effect on a material's rheological characteristics [22].

2.7.1 Viscosity

Viscosity is a critical parameter in the rheology study since it characterizes a fluid's resistance to flow. The greater the viscosity of the fluid, the more

external force must be applied to create flow (yield stress). For example, sirup has a high viscosity and needs more external force to flow, while water has a low viscosity and will flow easily. As a result, water is more easily displaced than sirup. In a primary cementing operation, a realistic displacement of fluids will contain fluids with a greater viscosity difference than presented in this thesis. The viscosity μ is defined as the ratio of shear stress τ to shear rate γ :

$$\mu = \frac{\tau}{\gamma} \tag{2.10}$$

Newtonian / Non-Newtonian

Newtonian or non-Newtonian rheological models are frequently applied to characterize fluid flow in the oil field. Newtonian fluid flow behavior is the simplest; fluid viscosity is the linear constant of proportionality between shear stress and shear rate at constant temperature and pressure. Newtonian fluids start flowing instantaneously, and shear stress increases with increasing shear rate. Numerous fluids, such as water, oil, gasoline, ethanol, and glycerin, behave as Newtonian fluids; their viscosity is determined only by the fluid's state and temperature. A plot of shear stress against shear rate for Newtonian fluids creates a straight line that passes through the origin of the plot coordinates, and the slope of the line is referred to as the fluid's Newtonian, or dynamic viscosity (Fig 2.9) [22]. The following equation expresses this relationship:

$$\tau = \mu \cdot \gamma \tag{2.11}$$

2.7 Rheology

The majority of fluids are non-Newtonian in nature. For example, drilling fluids and cement slurries are non-Newtonian. There is no proportionality constant between shear stress and shear rate for these fluids; their viscosity changes with varying shear rate. Apart from being pressure and temperature dependent, the viscosity of these fluids can either decrease with shear rate, in which case it is referred to as shear thinning, or increase with shear rate, in which case it is referred to as shear thickening [6]. Non-Newtonian fluids are further classified according to the models used to define them. The Bingham plastic, power-law, and Herschel-Bulkley models are the most relevant in drilling fluid technology. The majority of fluids do not fit to a single model accurately but mostly to a combination of models [22].

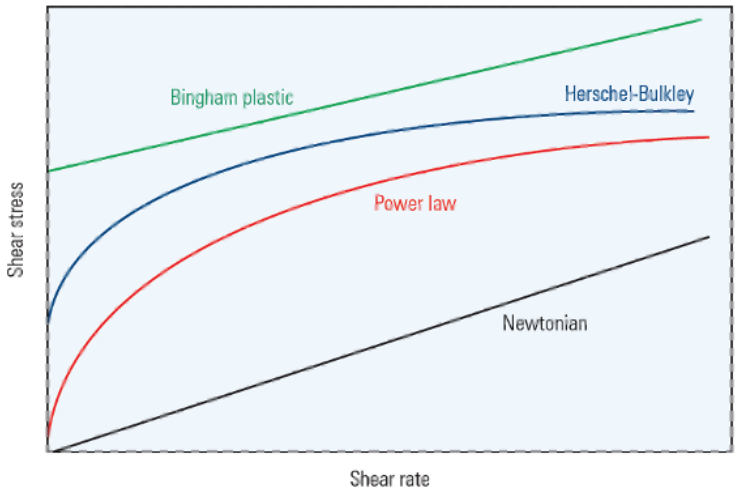

Figure 2.9: *Rheological models [22]*

While these experiments do not include the use of non-Newtonian fluids, it is crucial to note that such fluids will exhibit a different behavior and therefore may differ from the results obtained in the experiments described in this thesis.

2.8 Dimensionless numbers

In order to be able to model and scale the experiments, it is important to find the dimensionless numbers that are representative for flows in a eccentric annulus. In this section we will define some dimensionless parameters.

2.8.1 Reynolds number

The flow behavior of a fluid can be classified as laminar or turbulent. At large Reynolds number the inertial force is greater than the viscous forces, and consequently the viscous forces are incapable of preventing fluctuations when the flow is unpredictable and chaotic. However, at small Reynolds number the viscous forces are sufficient to overcome the inertial forces and is characterized by ordered, linear flow with no crossflow in axial and radial direction [19]. (Fig 2.10)

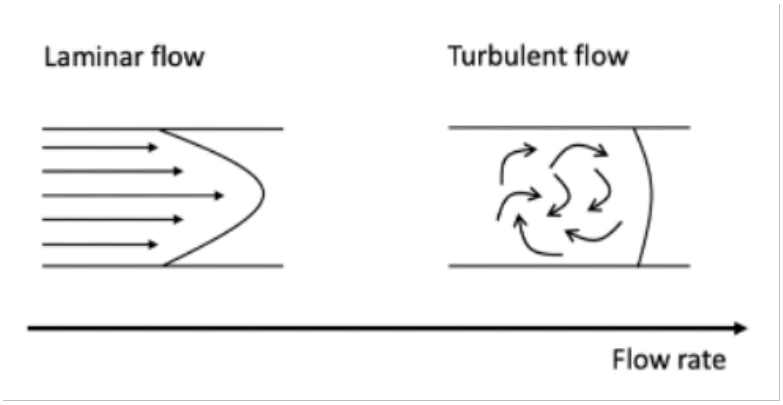

Figure 2.10: *Laminar and turbulent flow*

The flow behavior is described by the dimensionless parameter, the Reynolds number. For a Newtonian fluid in an annular geometry the formula is given by:

$$Re = \frac{\rho \cdot V \cdot D_h}{\mu} \tag{2.12}$$

Where ρ is the fluid density, V is the flow velocity, D_h is the characteristic/hydraulic diameter ($D_h = D_{outer} - D_{inner}$) and μ is the viscosity of the fluid. Although accurate Reynolds numbers for laminar, transitional, and turbulent flows are ideal, this is not the case in practice. This is because the transition from laminar to turbulent flow is also influenced by the degree to which the flow is disturbed by surface roughness, pipe vibrations, and flow variations. For a pipe, the various types of flow regimes are defined as follows in relation to the Reynolds number [19]:

Table 2.1: Different type of flow regimes depending on Reynolds number

Flow type	**Range of Reynolds number**
Laminar flow	Re $\leq$ 2300
Transitional flow	2300 $<$ Re $<$ 4000
Turbulent flow	Re $\geq$ 4000

2.8.2 Atwood number

The Atwood number is a dimensionless number that expresses the difference in density between two fluids that share an interface [23]. The formula used to define the Atwood number is:

$$At = \frac{\rho_2 - \rho_1}{\rho_2 + \rho_1} \tag{2.13}$$

Where ρ_2 is the displacing fluid (heavy) and ρ_1 is the displaced fluid (light) during conventional displacement.

2.8.3 Froude number

The Froude number (Fr) is a dimensionless quantity that expresses the ratio of inertia to gravity or buoyancy. The Froude number is stated in densimetric terms [24]:

$$Fr = \frac{V}{\sqrt{At \cdot g \cdot D_h}} \tag{2.14}$$

Where V is the fluid velocity, At is the Atwood number, g is the gravitational constant and D_h is the characteristic/hydraulic diameter. The Froude number is significant in fluid dynamics because it is used to calculate momentum transfer. Small values of the Froude number imply that the system is dominated by the effects of the density difference, i.e. buoyancy forces.

2.9 Scaling and Modelling

In physical research, it is desirable to establish a relationship between the parameters that describe the phenomenon being studied [25]. To save time and money, most experiments are conducted on a geometrically scaled *model* instead of the full-scale *prototype*. To achieve *similarity* between the model and the prototype, there are three essential conditions that must be fulfilled. The first condition is *geometric similarity*, which state that the

model must be identical to the prototype in shape but may be scaled by some constant factor. The second condition is *dynamic similarity*, which state that the forces in the model flow must be identical to the prototype flow, but be scaled by a constant factor. The third condition is *kinematic similarity*, which state that for each point in the model flow, the velocity must be identical to the velocity at the same place in the prototype flow, but scaled by a constant factor [26]. According to Barenblatt, the Buckingham Pi theorem can be defined as:
A physical relationship between some dimensional (generally speaking) quantity and several dimensional governing parameters can be rewritten as a relationship between a dimensionless parameter and several dimensionless products of the governing parameters; the number of dimensionless products is equal to the total number of governing parameters minus the number of governing parameters with independent dimensions [25, p.24]

$$\Pi = \Phi\left(\Pi_1, \ldots, \Pi_k\right) \tag{2.15}$$

Where Π is a dimensionless parameter. So to establish total similarity between the model and the prototype, each model's independent Π_m must be identical to the prototype's corresponding independent Π_p:

$$\Pi_{1,\ m} = \Pi_{1,p}\ ,\ \ldots,\ \Pi_{k,m} = \Pi_{k,p} \tag{2.16}$$

2.10 Flow governing equations

The fundamental governing equations of fluid dynamics—the continuity, momentum, and energy equations — are the foundation of fluid dynamics.

They are mathematical expressions of three fundamental physical principles [27]:

- Mass is conserved
- Linear momentum is conserved (Newton's second law)
- Energy is conserved (First law of thermodynamics)

The continuity equation describes mass conservation, whereas the Navier-Stokes equations describe liner momentum conservation. These physical principles are the cornerstone of computational fluid dynamics (CFD), and are used to solve fluid flow numerically [27].

2.10.1 Continuity equation

The continuity equation is founded on the fundamental physical principle of mass conservation. The continuity equation is the statement of mass conservation. A continuity equation is a mathematical expression that describes the movement of a given quantity and cam be defined as [28]:

$$\frac{\partial \rho}{\partial t} + \nabla \cdot (\rho \vec{u}) = 0 \tag{2.17}$$

Where ρ is density, t is time and $\vec{u}$ is the flow velocity vector.

However, if we consider an incompressible and homogeneous fluid, the continuity equation can be simplified and defined as:

$$\nabla \cdot \vec{u} = 0 \tag{2.18}$$

2.10.2 Navier-Stokes equation

The Navier-Stokes equation is a partial differential equation that describe the flow of viscous liquids by utilizing Newton's second law [29]. The Navier-Stokes equation is a mathematical expression for momentum conservation. If we consider an incompressible and homogeneous fluid the Navier-Stokes can be defined as:

$$\hat{\rho}_i \left(\frac{\partial \hat{\vec{u}}}{\partial \hat{t}} + \left(\hat{\vec{u}} \cdot \hat{\nabla} \right) \hat{\vec{u}} \right) = -\hat{\nabla} \hat{p} + \hat{\mu} \cdot \hat{\nabla}^2 \cdot \hat{\vec{u}} + \hat{\rho}_i \hat{\vec{g}} \tag{2.19}$$

Where u is the fluid velocity, μ is the fluid dynamic viscosity and p is the fluid pressure, and ρ_i is the fluid density:

$$\hat{\rho}_i = \overline{\hat{\rho}}(1 + \Phi_i A t) \tag{2.20}$$

Where the subscript i is whether it is the displacing or displaced fluid, Φ_i is +1 for displacing fluid ($i = 1$) and -1 for displaced fluid ($i = 2$), and $\overline{\hat{\rho}}$ is the average density.

The first term in equation 2.19 denotes inertial forces, the second term denotes pressure forces, the third term denotes viscous forces, and the fourth term denotes external forces. External forces are represented by hydrostatic pressure in this case [30].

2.10.3 Navier-Stokes with dimensionless numbers

In order to fit different dimensionless numbers, the Navier-Stokes equation can be rearranged (See Appendix B). By introducing characteristic velocity and length scale, we obtain Navier-Stokes on this form:

$$(1 + \Phi_i At)\, Re \left(\frac{\partial \vec{u}}{\partial t} + \left(\vec{u} \cdot \vec{\nabla} \right) \vec{u} \right) = -\vec{\nabla} p' + \nabla^2 \vec{u} + \Phi_i \frac{Re}{Fr^2} \vec{e}_g \qquad (2.21)$$

Where $\vec{e}_g$ is the unit vector in the direction of $\vec{g}$. As seen from the final equation, the dimensionless parameters that govern the flow are as follows: Atwood number, Reynolds number and Froude number [31].

Chapter 3

Methodology

3.1 Experimental setup

A schematic representation of the experimental setup is given in figure 3.1. Experiments were conducted in a well-flow test loop to investigate the displacement process during annular cementing. The experiment consists of a long outer pipe made from Lexan. It is less shiny than acrylic and can handle more impact. Lexan is hard to crack so that it will withstand the vibration. The outer pipe surrounds an inner pipe made of stainless steel. The annulus dimensions are r_o= 35.0 mm, r_i= 25.3 mm and a length of 151.6 cm. This leaves the annular space to be 9.75 mm when the inner pipe is concentric. The inner pipe is mounted in such a way that it is adjustable. By turning the eccentricity adjustment, the position of the inner pipe can be changed relative to the fixed outer pipe to create the desired eccentricity. The flow loop consists of Verderflex Rollit 25 centrifugal pump that first supplies the annulus with displaced fluid, followed by displacing fluid. A Y-coupling on the inlet of the pump regulates this. The flow rate is controlled by a switch that is varying the frequency on the pump. A conductivity meter (JUMO CTI-500) is mounted on the outlet to ensure that the displacement is fully achieved.

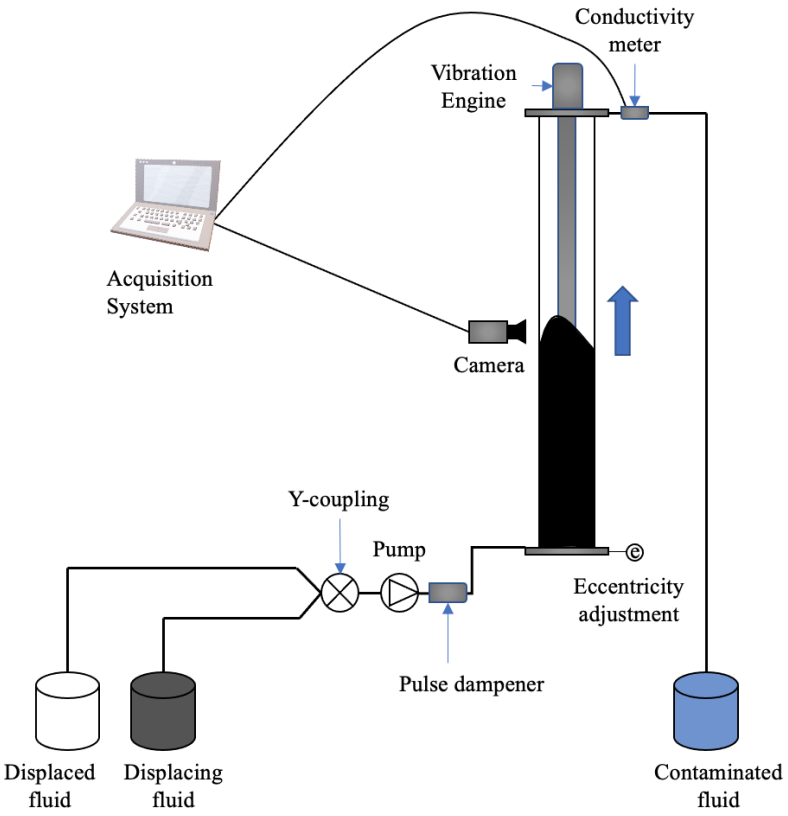

Figure 3.1: *Schematic of the experimental setup*

3.1.1 Scaling

Numerous parameters affect the displacement process during primary cementing. An experimental examination covering all aspects of the process would be a massive task. As a result, it was necessary to restrict the number of parameters that may be varied during the testing. In order to facilitate comparisons between displacement processes in the laboratory and in field case, the laboratory experiments must be carefully scaled to achieve similarities. The *geometrical similarity* on the test-rig was decided by the company which donated the rig to us. They scaled the rig to the

field case where there is a 7 5/8 inch hole with a 5 1/2 inch casing. This gives the ratio 1.39. This was a complete construction and the geometrical dimensions were fixed when we received the test-rig as shown in Fig 3.2

Figure 3.2: *The test-rig*

The geometrical dimensions for the experimental setup are listed below:

Table 3.1: Geometrical dimensions for the experimental setup

Parameter	**Symbol**	**Value**
Inner diameter of cylinder	ID	70.0 mm
Outer diameter of inner pipe	OD	50.5 mm
Hydraulic diameter	D_h	19.5 mm
Height of cylinder	L	1516 mm

Next, we considered the *dynamic similarity*. By utilizing the rearranged form of Navier-Stokes, we can obtain the dimensionless numbers that governs the flow in this experiment. For our scaling, we received some real field-case data. While it would be ideal to be able to pick fluids that match given dimensionless parameters, this is quite challenging in practice, especially when working with transparent and relatively inelastic fluids. The field data provided some dimensionless numbers that we then needed to match. We decided to focus on Re and Fr, which we regard as the most important dimensionless numbers. Even though we were limited to Newtonian fluids, we managed to fit the most important dimensionless numbers. This is shown in table 3.2.

Table 3.2: Field values vs. Experimental values

Parameter	**Field Values**	**Experimental Values**
ρ_2 $[kg/m^3]$	1003	998
ρ_1 $[kg/m^3]$	1920	1111
Q [L/min]	600	6
μ_2 [Pa·s]	0.0010	0.0011
μ_1 [Pa·s]	0.19	0.00242
$Re_{displacing}$	334.91	485.48
$At_{displacing}$	0.31	0.05
$Fr_{displacing}$	0.557	0.536
$Re_{displaced}$	33241.85	989.13
$Fr_{displaced}$	0.557	0.536

As seen from the table above, the Reynolds number for the displacing is off by 150. Nonetheless, the experimental value is well within the range of laminar flow. The Reynolds number for the displaced fluid in the field

is turbulent, but the experimental value is within the laminar regime. The difference in Fr is negligible, so we have obtained similarity in 2/3 of the dimensionless numbers for the displacing fluid. This is as field realistic we will be able to make the experiments with Newtonian fluids.

3.1.2 Selection of fluids

In this experiment, fresh water is used as the displaced fluid. Fresh water are considered to be an incompressible fluid with constant viscosity. To achieve the desired density and viscosity of the displacing fluid, we added sugar and salt as weighting agents. Additionally, the displacing fluid were dyed with black ink, at a concentration of 1ml ink per 1000ml water. This is done to visually separate the displacing fluid and the displaced fluid by creating a clear interface between the two fluids. To achieve the experimental values presented in table 3.2, we changed the characteristics of the displacing fluid by adjusting the concentration of sugar and salt to 25% and 1%, respectively. Due to covid-19 and a lot of activity at the facility, we decided to keep the characteristic of the displacing fluid constant throughout all the experiments. The final characterization of the displacing fluid and the displaced fluid are listed below in table 3.3:

Table 3.3: Characterization of test fluids
(Salt is NaCl; Sug is sugar)

Displacing fluid				Displaced fluid			
Fluid	Concentration (weight of water, %)	ρ_1 (kg m^{-3})	μ_1 (Pa s)	Fluid	Concentration (weight of water, %)	ρ_2 (kg m^{-3})	μ_1 (Pa s)
Fresh water	25% Sug, 1% Salt	1111	0.00242	Fresh water	-	998	0.0011

3.2 Equipment

3.2.1 Conductivity transmitter

To ensure that the displacement is fully achieved, we mounted a JUMO CTI-500 inductive conductivity and temperature transmitter on the outlet of the flow-loop. The probe is shown in figure 3.3.

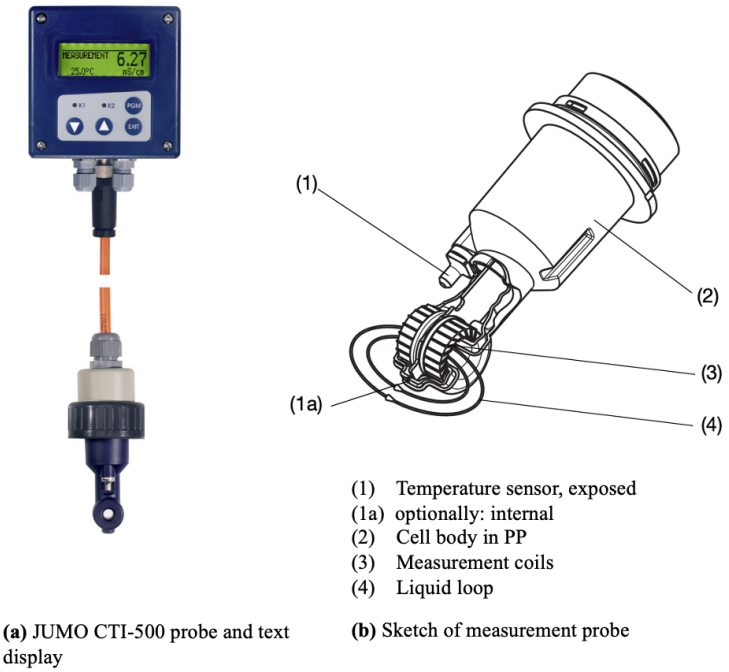

(a) JUMO CTI-500 probe and text display

(b) Sketch of measurement probe

Figure 3.3: *JUMO CTI-500 conductivity transmitter*

The conductivity was calibrated at different concentrations of NaCl in fresh water. This is listed in table 3.4.

Table 3.4: Conductivity measurements of fresh water with varying concentration of NaCl

Concentration NaCl (by weight of water)	Conductivity of fresh water (mS/cm)
1%	19
3%	48
5%	76

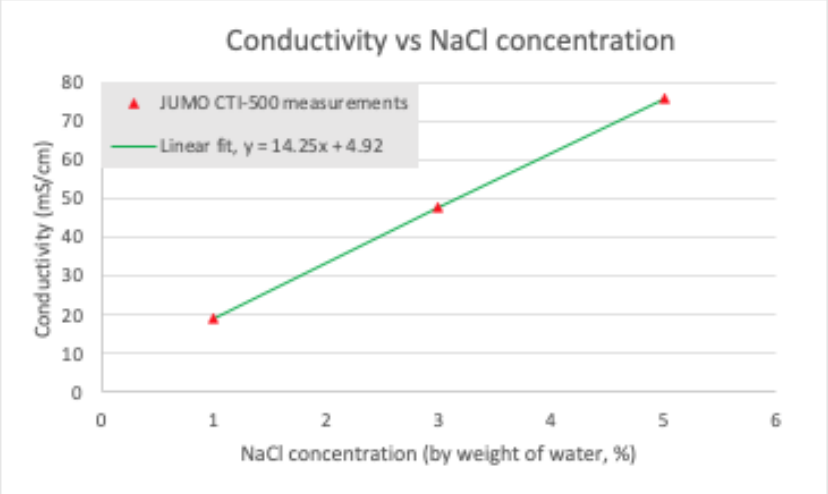

Figure 3.4: *Conductivity measurements from table 3.4 and a linear fit*

As seen from the figure above, there is a linear fit. This indicates a 1:1 ratio between the concentration and the conductivity. By dissolving sugar in the displacing fluid, the measured conductivity does not match the theoretical conductivity. This is because the conductivity is controlled by the ion concentration and the number of charges per ion. The measured conductivity of the displacing fluid was found to be between 10.00 and 10.50.

3.2.2 Flow meter

A new flow meter was purchased for this project, but due to a malfunction, we were required to manually determine the desired flowrate of 6L/min. This

was accomplished by setting the pump to a specific frequency and then timing how long it took to pump 2L of water through the flow-loop. After achieving a flowrate of 6L/min, we repeated the test four times to confirm that it was accurate. This was done in order to remove the possibility of human error while interacting with the stop watch.

3.2.3 Camera setup

The camera used for this project is a Nikon D7500. It records video at 60 frames per second, and by using MATLAB, the movie is split into images. Behind the test-section there is placed a white cardboard to better distinguish the displaced fluid (transparent) and the displacing fluid (dyed in black ink). In addition, extra lighting were provided by two LED-lamps behind the camera setup. Due to problems with bubbles of air entering the annulus and limited amount of displacing fluid, the camera was set up in such a way that it covers 35cm of the test-section. However, the conductivity measurements covers the whole test-section.

3.2.4 Rheometer

For this project, a Anton Paar MCR 301 rheometer was used to measure the viscosity of the fluids. This is a rotational rheometer and they are based on the principle that the torque required to rotate an object in a fluid is a function of the viscosity of that fluid. They determine the torque necessary to rotate a disk or cone at a specified speed. This rheometer have a narrow-angled cone descending down on a flat plate, leaving a gap on 0.0052mm. At any given rotating speed, the system ensures a constant shear rate between the geometries. The viscosity are determined using the shear stress (derived

from the torque) and shear rate (from the angular velocity). This is done by the computer and we can easily read the viscosity from the computer screen.

3.2.5 Density meter

To measure the density of the fluids, a Anton Paar DMA 4500 M was used for this project. By filling the u-shaped with fluid the measurement can begin. The on-screen display shows the u-tube and it is important to ensure that there are no air-bubbles. The density meter operates on the oscillating U-tube principle; a sample of fluid is injected into a U-shaped glass tube, and the density is measured by vibrating the glass tube at a specific frequency. The frequency is related to the sample's density, and by identifying the fluid's characteristic frequency, the density are determined. This is done automatically and the density is displaced on the screen.

3.2.6 Vibration tool

On the test-rig, the vibration tool has a strong lateral movement paired with a modest oscillating movement. Controlling the intensity is accomplished using a control placed on the apparatus. It ranges from 0Hz to 16.5Hz. Although the test equipment was fastened, HSEQ indicated that it was not possible to exceed 10Hz in a vertical configuration.

3.3 Experimental plan

The experimental plan are presented in table 3.5. For these experiments the inclination of the test-rig is set to vertical. The rheological characteristic of the two fluids are kept constant. The flowrate are also kept constant at 6L/min throughout all the experiments. (As listed in table 3.2). The

parameters that are not kept constant, are eccentricity and the intensity of the vibration. The influence of eccentricity and vibration were studied in these experiments.

Table 3.5: Experimental plan.
Varying eccentricity and vibration

Run	Eccentricity	Vibration intensity (Hz)
1	0	0, 2.5, 5, 10
2	0.46	0, 2.5, 5, 10
3	0.82	0, 2.5, 5, 10

Chapter 4

Experimental Results and Discussion

4.1 Validating ELF-rules

Before displaying the visual representations of the various experiments, we validate the ELF-rules presented in the theory section of this thesis. This is done to determine whether or not the criteria for a steady-state displacement are met.

Firstly, in our experiments, the displacing fluid is 1.11 times more dense than the displaced fluid. This indicates that the fluids satisfy the density hierarchy criteria of the first rule (Eq. 2.5).

When Newtonian fluids are considered, and the flow rate is constant, the friction pressure can be simplified to the viscosity. In our experiments, the ratio of displacing to displaced fluid viscosity is 2.2. Thus, the friction pressure hierarchy criteria in the second rule (Eq. 2.6) is also satisfied.

Due to the fact that this experiment only consists of Newtonian fluids, the third rule involving gel strength becomes invalid (Eq. 2.7). Lastly, the fourth and final rule (Eq. 2.8) is also satisfied. Even for the most eccentric experiment.

This concludes that all the ELF-rules criteria for a steady-state displacement are satisfied.

4.2 Uncertainties

As mentioned in section 3.2.2, we had to manually validate the flowrate. This was tested without vibration. The pump are set to a given power output, and not a specific flowrate. This flowrate may have been disturbed by the vibration in the annulus. Without a flow-meter, we will never be certain of the flowrate during vibration.

Another uncertainty is the problem of bubbles of air entering the annulus, as mentioned in section 3.2.3. No matter how long we circulated fresh water, small bubbles of air nearly always entered the annulus. However, to the best of our ability, the recorded experiments were conducted without these bubbles of air.

Additionally, the absence of a fish tank surrounding the circular pipe is also an uncertainty. Optical distortion is introduced into images of circular pipes. As a result, the images do not accurately depict what is actually happening.

After each experiment, the rig was flushed with fresh water to clean out the pipes, but residual displacing fluid may have managed to remain in the pipe, affecting the properties of the displaced fluid in the subsequent experiment. However, the amount of displacing fluid remaining after cleaning is assumed to be negligible and will have no significant effect on the subsequent experiment.

4.3 Visualization of displacement

For the purpose of illustration and a better understanding of the images, the narrow and wide side of the annuls are pointed out in Fig 4.1. For each experiment, the camera is positioned in the same location. In these images, the pipe is filled with fresh water. The narrow side is located on the right side, whereas the the wide side is located on the left side of the images.

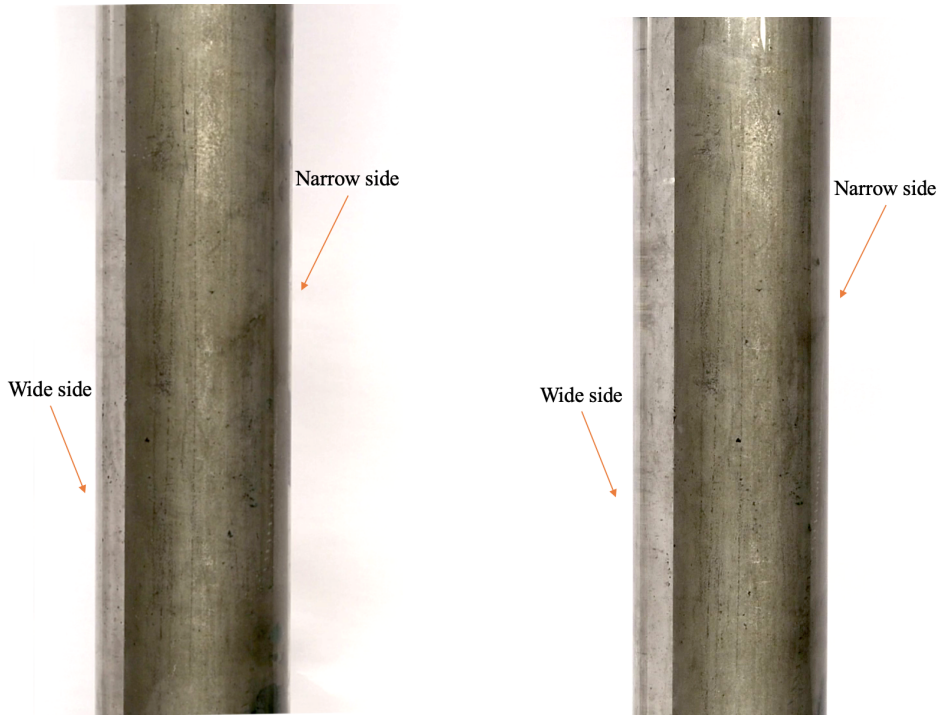

(a) Ecc=0.46 (b) Ecc=0.82

Figure 4.1: *Illustration of the narrow and wide side*

4.4 Effect of eccentricity

In this section, it is studied how the change in eccentricity influence the displacement. As the eccentricity increases we can see that the experimental results matches according to the theory. The displacing fluid will choose the path of least resistance and therefore favorite the wide part of the annulus. But as mentioned above, the ELF-criteria are satisfied, so we get a steady-state displacement.

For the experiments without vibration, I tried to make some plots of the front by coding a edge-detection program. This is done by first editing the pictures to grey-scale, then adjusting the contrast. Then I put the value for black = 1 and white = 0. Then I put the value for interface at 0.95. This is done because the interface is never sharp in a miscible displacement. Due to the uncertainty regarding the glass mentioned above, the curves for the concentric and medium eccentricity does not look so good. Nonetheless, we can clearly see how the front develop with increasing eccentricity. This matches accordingly with the theory of displacements in an eccentric annulus.

The results are presented as a series of pictures that displays the displacement front with varying eccentricity, starting at concentric. Below each series, the edge-detection plot is also presented. For the purpose of comparison with the experiments with vibration, the conductivity measurements curves for non-vibrating experiments are presented in the end of this section.

4.4 Effect of eccentricity

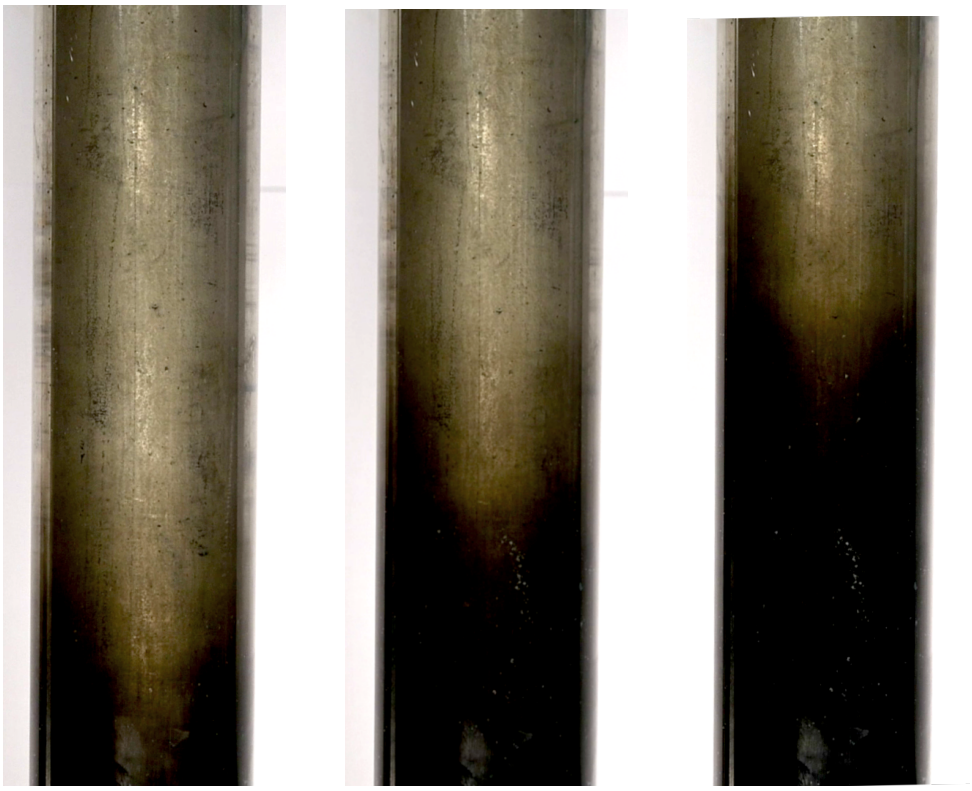

(a) (b) (c)

Figure 4.2: *Displacement in a concentric annulus*

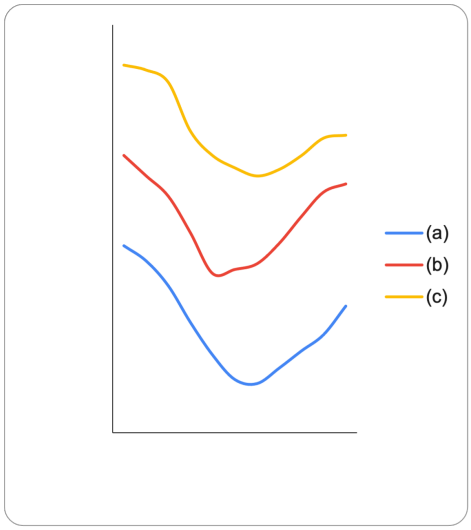

Figure 4.3: *Edge-detection coding of front, concentric*

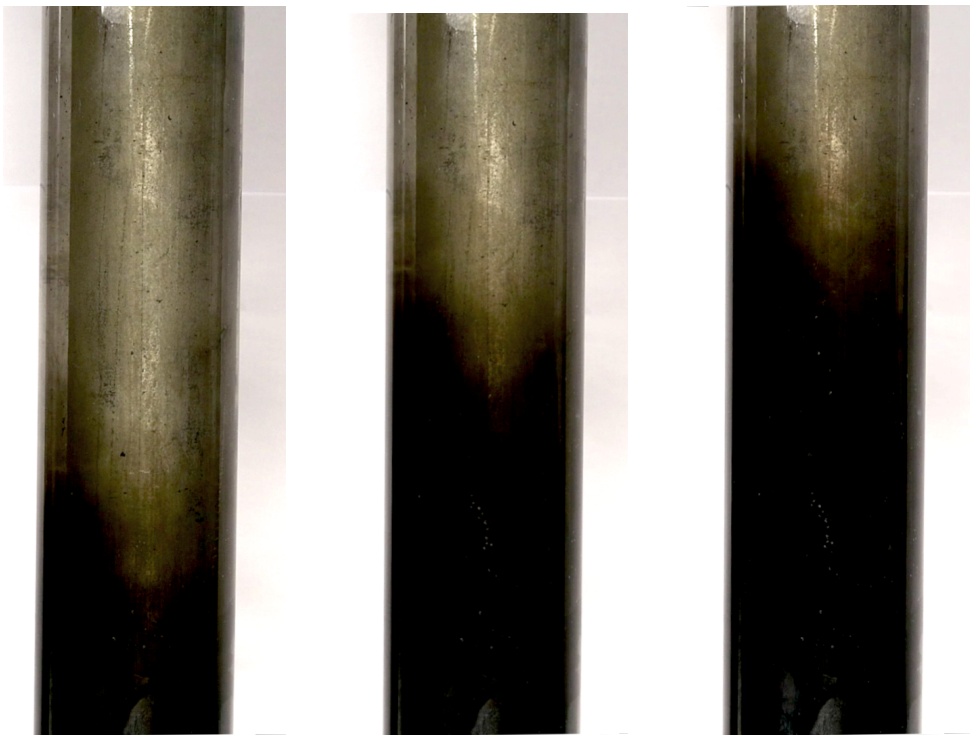

(a) (b) (c)

Figure 4.4: *Displacement in a medium eccentric annulus*

Ecc=0.46

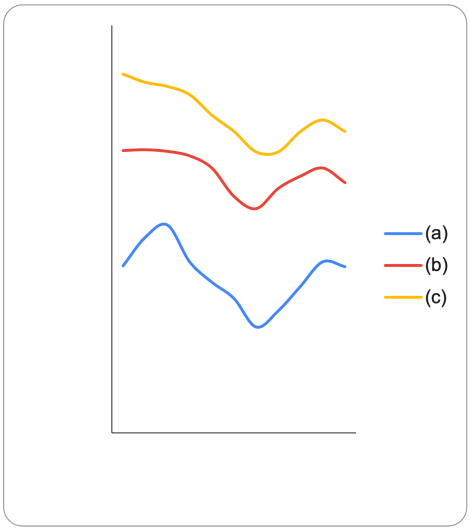

Figure 4.5: *Edge-detection coding of front, medium eccentricity*

4.4 Effect of eccentricity

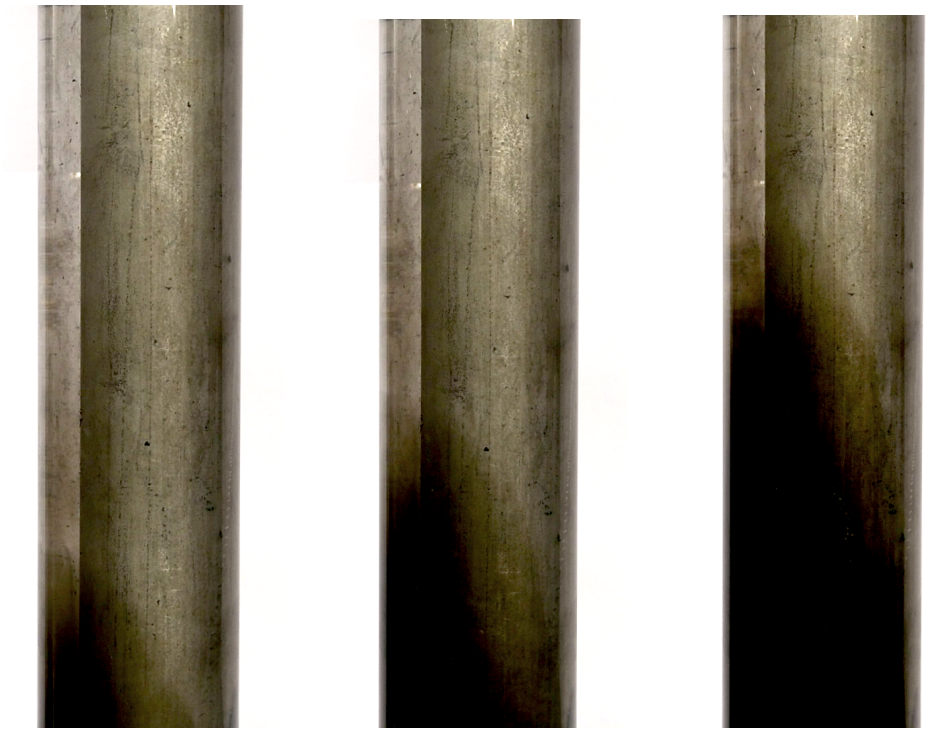

(a) (b) (c)

Figure 4.6: *Displacement in a high eccentric annulus*

Ecc=0.82

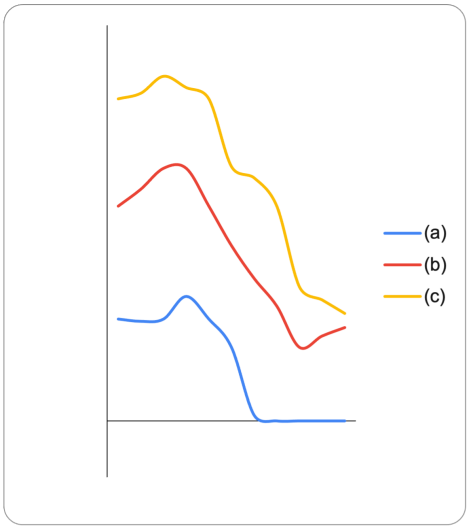

Figure 4.7: *Edge-detection coding of front, high eccentricity*

4.4 Effect of eccentricity

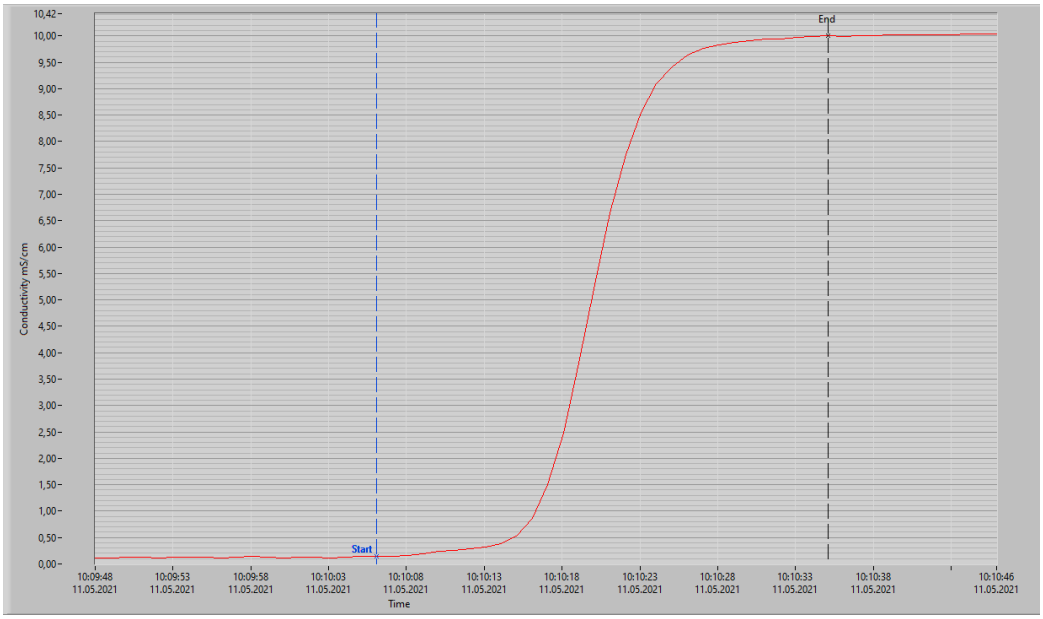

Figure 4.8: *Conductivity measurements for concentric*

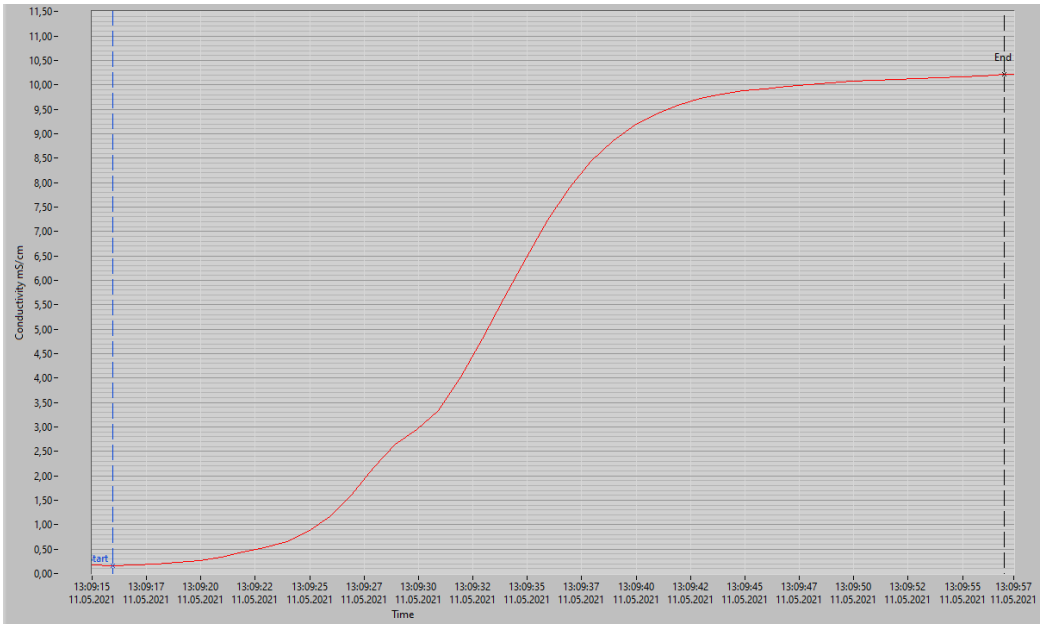

Figure 4.9: *Conductivity measurements for medium eccentricity*

Ecc=0.46

4.4 Effect of eccentricity

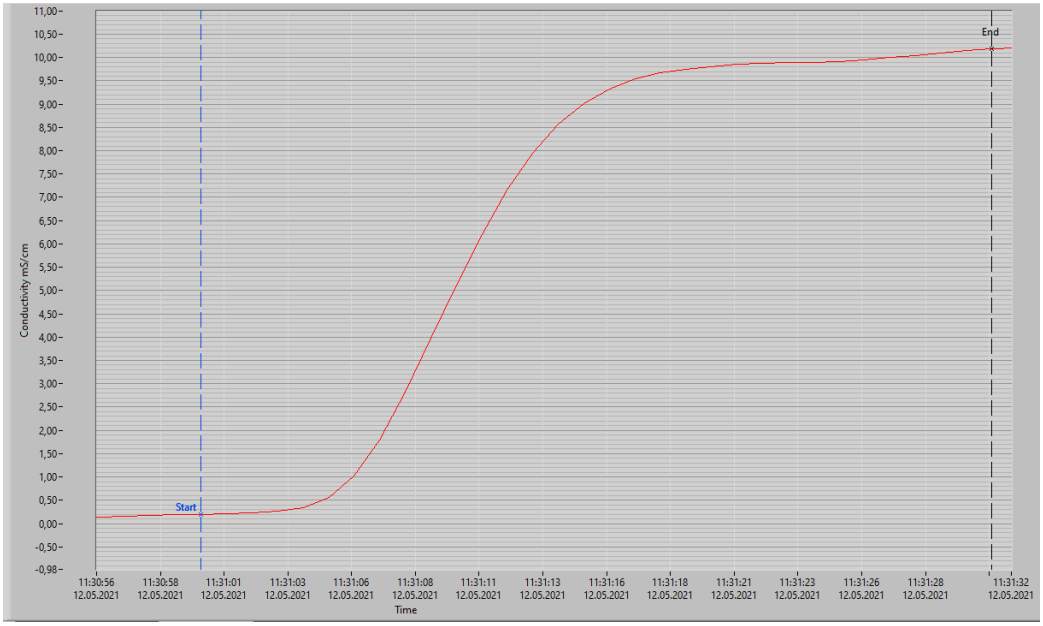

Figure 4.10: *Conductivity measurements for high eccentricity Ecc=0.82*

As seen from the displacement efficiency curves above, the one with high eccentricity starts to flatten out earlier compared to the one that displays a concentric annulus (Fig 4.8). This is due to some residual water on the narrow side of the annulus as shown in figure 4.11.

Figure 4.11: *Residual water during displacement when Ecc=0.82*
Picture taken from the side (right side in comparison of the other pictures)

4.5 Effect of vibration

In this section, it is studied how the change in vibration-intensity influence the displacement process. Due to the difficulty of illustrating the vibration with images, this section will have a greater emphasis on the conductivity measurement curves.

It was discovered that the vibration intensities of 2.5Hz and 5Hz had an insignificant effect, or no effect at all. Similarly, there were not seen any significant effect of vibration in the concentric annulus, neither when the eccentricity was 0.46. So these experiments will only be presented once. As a result, only the most significant discoveries will be addressed in this section. The rest of the results are included in Appendix A. The key results are presented by first comparing the conductivity measurements curves, then presenting the visualization of the displacements at the end of this section.

4.5 Effect of vibration

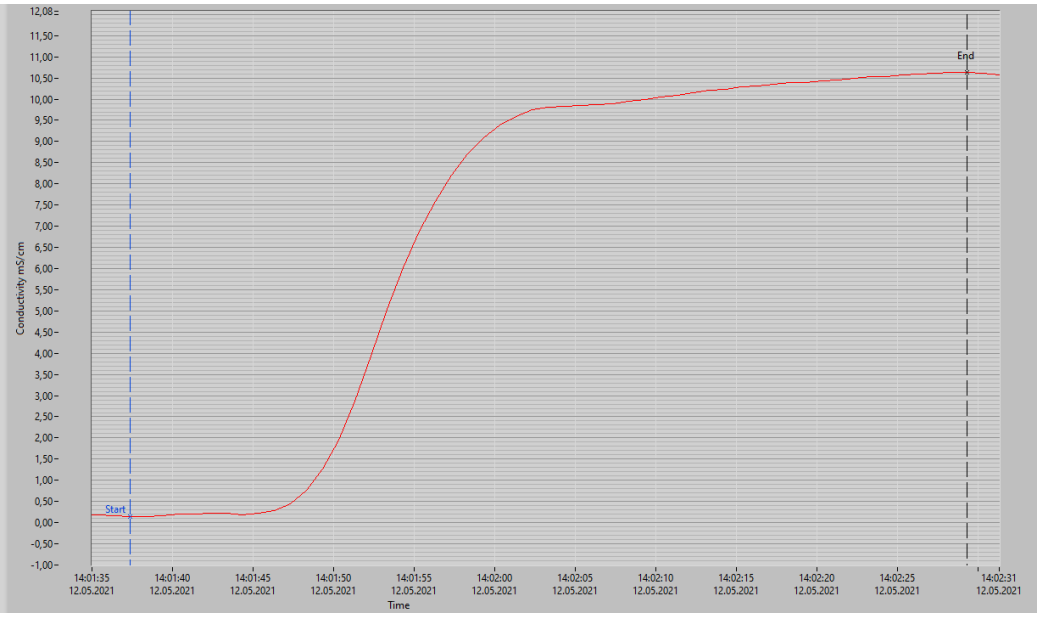

Figure 4.12: *Conductivity measurements for Ecc=0.82, 10Hz*

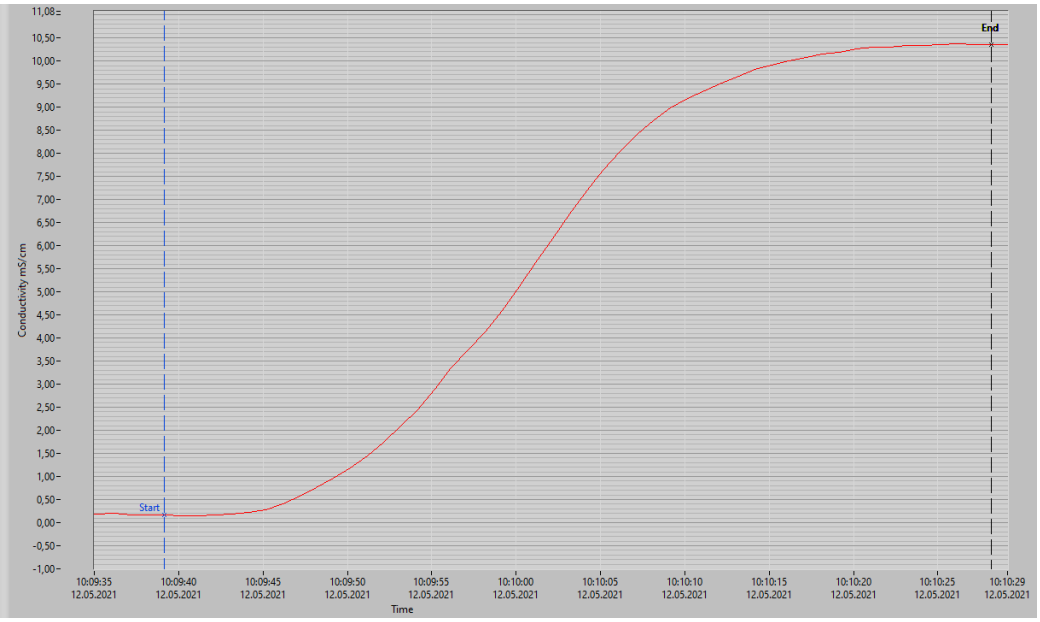

Figure 4.13: *Conductivity measurements for Ecc=0.46, 10Hz*

4.5 Effect of vibration

The displacement of the annulus with an eccentricity of 0.82 in combination with 10Hz vibration takes 20 seconds longer than the non-vibrating experiments. For the experiment with eccentricity of 0.46 the displacement takes 13 seconds longer. This could be a result of the uncertainty regarding the manual flowrate mentioned in section 4.2. Another possibility could be that when exposed to high intensity vibration, the front velocity profile experiences radial forces that results in flattening of the velocity profile.

Next, the visualization will be presented. The first series will be of 0.46 eccentricity and 10Hz vibration. This is done to show that there was an insignificant effect, or no effect at all, when it was performed with this eccentricity. Similarly, there will be shown one example of 2.5Hz and 5Hz. Then the experiment regarding 0.82 eccentricity and 10Hz will be be presented. Here, we can see that the front exhibits a more piston-like behavior. On the wide side, the front does not propagate as extreme as it does in other experiments with this eccentricity. By causing circumferential flow of the fluid, this vibration enables fluid to be transferred from the narrow side to the wide side. As a result, the 10Hz vibration intensity contributes to successful removal of the residual water column indicated in Fig 4.11.

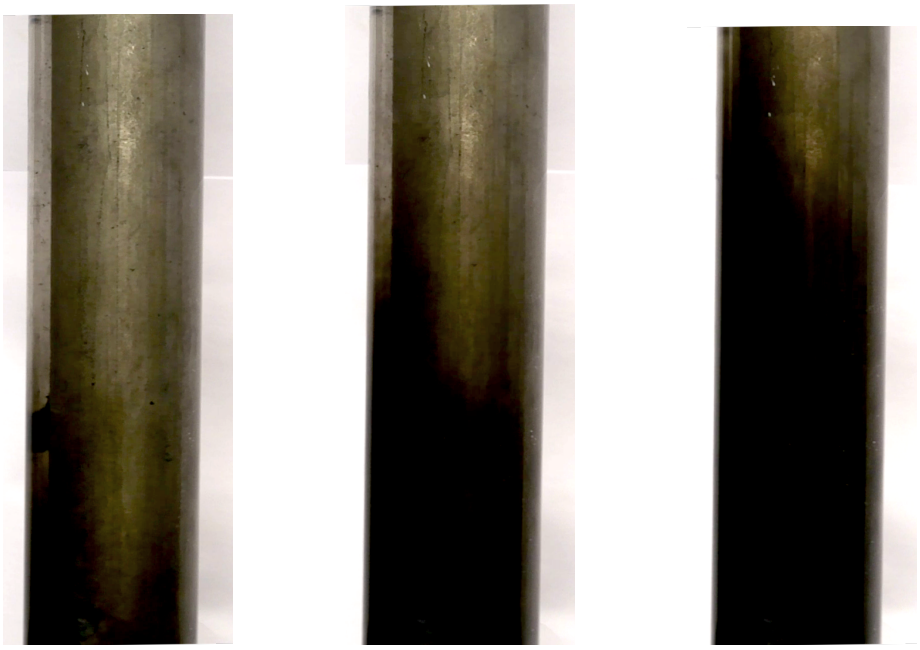

(a) (b) (c)

Figure 4.14: *Visualization of displacement: Ecc=0.46, 10Hz*

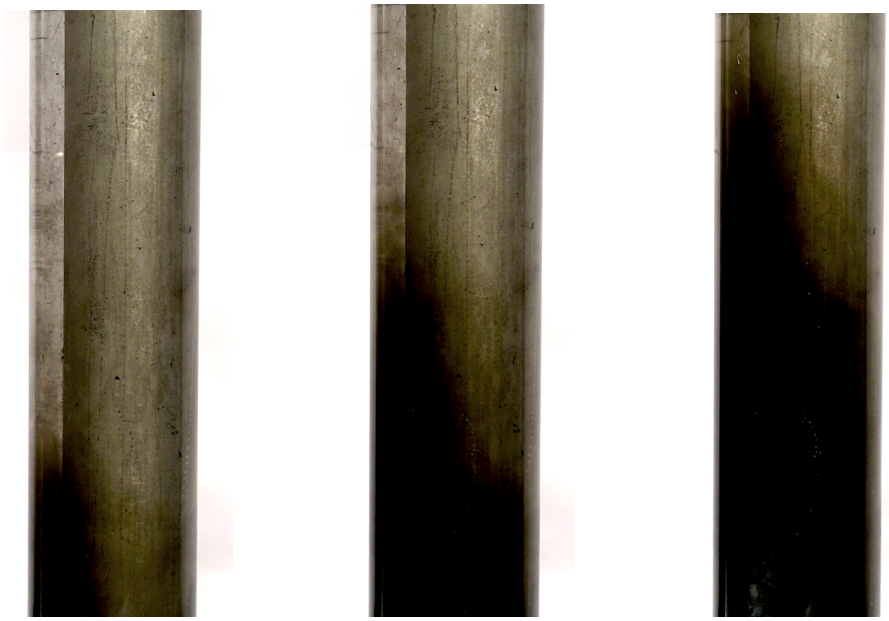

(a) (b) (c)

Figure 4.15: *Visualization of displacement: Ecc=0.82, 2.5Hz*

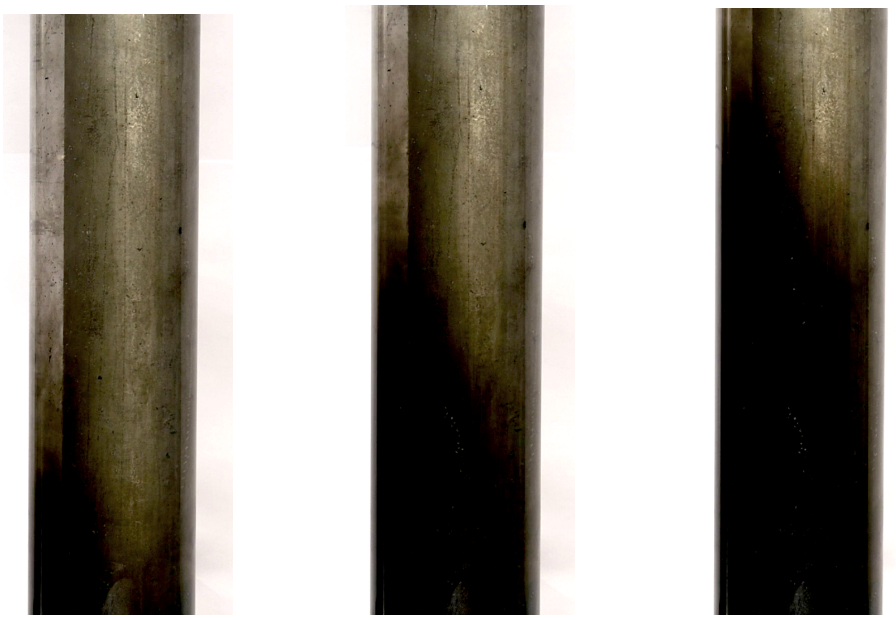

(a) (b) (c)

Figure 4.16: *Visualization of displacement: Ecc=0.82, 5Hz*

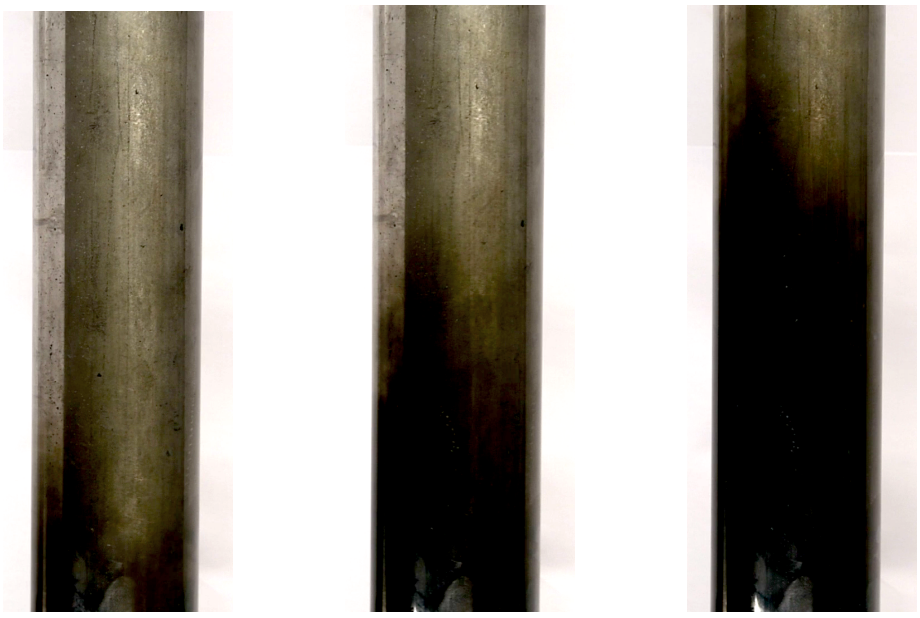

(a) (b) (c)

Figure 4.17: *Visualization of displacement: Ecc=0.82, 10Hz*

Chapter 5

Conclusion

It is absolutely essential to emphasize that these experiments serve as benchmark tests for this vibration tool. Experiments with no vibration and increasing eccentricity substantiate the theory well. The tool had no significant effect on the results obtained with low and medium vibration intensities. However, when the vibration is set to a high frequency, such as 10Hz, we observe a significant effect. Displacement improves and becomes more efficient when exposed to 10Hz vibration. It also manages to eliminate the residual water column on the narrow side of the annulus. That being said, this type of vibration is not suitable for use in the field because it can damage the equipment and the surroundings. As this is a benchmark experiment, we will now make some recommendations for further research.

5.1 Recommendation for further work

In these experiments, only Newtonian fluids were used. The displacing fluid and the displaced fluid were both incompressible, homogeneous and miscible. It would be interesting to introduce polymers to the fluids in order to alter its viscosity and thus study the effect of viscosity. By introducing non-Newtonian fluids, the experiments will become even more field realistic. Non-Newtonian fluids have the ability to better replicate the characteristics of spacer/brine/cement (gel strength etc). It would also be interesting to investigate the effect of a greater density difference.

Another interesting thing to study further would be to make the inner pipe obtain a rotational movement instead of heavily lateral.

In the field, there is often control-lines attached to the pipe. These experiments were conducted without control-lines, so it would be interesting to study if the control-lines will have any effect of the displacement. The test-rig arrived with control-lines attached, so this can easily be studied since they are already fabricated and ready to mount on the rig.

It would be interesting to see if there is any critical point of inclination were the tool starts to show significant results. The same applies for the intensity of the vibration. If we get to know the amplitude, we can study if there is any critical amplitude that shows significant result.

Improvements to the experimental setup

Lastly, some improvements to the experimental setup will be provided:

- Install a flow-meter
- Install a tank with square cross-section around the circular pipe to reduce optical distortion. Fill with glycerin.
- Make the hoses as short as possible, so the risk of bubbles of air entering the annulus is minimized.
- Improve the fastening of the rig, so we can safely achieve higher vibration intensities.
- Build a construction that surrounds the test-rig with curtains to block out external lightning.

References

[1] M. Höök, S. Davidsson Kurland, S. Johansson, and X. Tang, "Decline and depletion rates of oil production: A comprehensive investigation," *Philosophical transactions. Series A, Mathematical, physical, and engineering sciences*, vol. 372, Jan. 2014. DOI: 10.1098/rsta.2012.0448.

[2] Petrowiki, *"glossary: Economic limit"*. [Online]. Available: https://petrowiki.spe.org/Glossary:Economic_limit, (accessed: 12.03.2021).

[3] M. Höök, B. Söderbergh, K. Jakobsson, and K. Aleklett, "The evolution of giant oil field production behavior," *Natural Resources Research*, vol. 18, pp. 39–56, 2009. DOI: 10.1007/s11053-009-9087-z.

[4] J. O. Spieler and T. M. Øia, *P&a - well statistics*, Oct. 2015. [Online]. Available: https://www.norskoljeoggass.no/globalassets/dokumenter/drift/presentasjonerarrangementer/plug--abandonment-seminar-2015/03---well-statistics-uis-students-spieler-og-oia.pdf.

[5] *Cement Placement with Tubing Left in Hole during Plug and Abandonment Operations*, SPE/IADC Drilling Conference and Exhibition, Mar. 2016. DOI: 10.2118/178840-MS.

[6] E. B. Nelson and D. Gulliot, *Well Cementing*, 2. ed. Sugar Land, Texas: Schlumberger, 2006.

[7] A. Maleki and I. Frigaard, "Primary cementing of oil and gas wells in turbulent and mixed regimes," *Journal of Engineering Mathematics*, vol. 107, no. 1, pp. 201–230, 2017. DOI: 10.1007/s10665-017-9914-x.

[8] F. Thom, P. Angell, N. Greig, N. Robertson, and H. Hogg, "Case study for rig-less subsea well abandonment," in *SPE/ICoTA Well Intervention Conference and Exhibition*, D021S013R003. DOI: 10.2118/199866-ms. [Online]. Available: https://doi.org/10.2118/199866-MS.

[9] International Association of Oil & Gas Producers, "Overview of international offshore decommissioning regulations - wells plugging & abandonment," IOGP, Report Report no. 585, Jul. 2017.

[10] Standards Norway, *NORSOK Standard D-010 - well integrity in drilling and well operations*, revision 4. Lysaker, 2013.

[11] Oil and Gas UK, "Guidelines for the abandonment of wells," *Oil and Gas UK*, 2015.

[12] S. Malekmohammadi, M. Carrasco-Teja, S. Storey, I. A. Frigaard, and D. M. Martinez, "An experimental study of laminar displacement flows in narrow vertical eccentric annuli," *Journal of Fluid Mechanics*, vol. 649, pp. 371–398, 2010. DOI: 10.1017/S0022112009993508.

[13] D. Smith, *Cementing*. H.L. Doherty Memorial Fund of AIME, Society of Petroleum Engineers, 1987. [Online]. Available: https://books.google.no/books?id=_p1gtAEACAAJ.

[14] *Dynamic Cementation: A Solution to Well Integrity Problems*, vol. All Days, SPE/IADC Drilling Conference and Exhibition, SPE-163459-MS, Mar. 2013. DOI: 10.2118/163459-MS.

[15] *Are Current Casing Centralization Calculations Really Conservative?* Vol. All Days, SPE/IADC Drilling Conference and Exhibition, SPE-112725-MS, Mar. 2008. DOI: 10.2118/112725-MS.

[16] H. J. Skadsem and S. Kragset, "Effect of buoyancy and inertia on viscoplastic fluid–fluid displacements in a regular and an irregular eccentric annulus," *Journal of Energy Resources Technology*, vol. 143, no. 6, 2020, ISSN: 0195-0738. DOI: 10.1115/1.4048529.

[17] *Optimization of Spacer Rheology Using Neural Network Technology*, vol. All Days, SPE/IADC Drilling Conference and Exhibition, Feb. 2002. DOI: 10.2118/74498-MS.

[18] Wikipedia, *Hagen-poiseuille equation*, 2021. [Online]. Available: https://en.wikipedia.org/wiki/Hagen-Poiseuille_equation#Poiseuille_flow_in_an_annular_section (visited on 05/26/2021).

[19] Y. A. Çengal, J. M. Cimbala, and R. H. Turner, *Fundamentals of thermal-fluid sciences*, Electronic Book, 2017.

[20] S. Pelipenko and I. A. Frigaard, "Visco-plastic fluid displacements in near-vertical narrow eccentric annuli: Prediction of travelling-wave solutions and interfacial instability," *Journal of Fluid Mechanics*, vol. 520, pp. 343–377, 2004, ISSN: 0022-1120. DOI: 10.1017/S0022112004001752.

[21] "Steady displacements for conventional and reverse circulation primary cementing," Unpublished Work, 2019-2023.

[22] I. M. Færgestad, "The defining series - rheology," *Oilfield Review*, 2016. [Online]. Available: https://www.slb.com/-/media/files/oilfield-review/defining-rheology.ashx.

[23] "Atwood number," in *Encyclopedia of Microfluidics and Nanofluidics*, D. Li, Ed. Boston, MA: Springer US, 2008, pp. 56–57. DOI: 10.1007/978-0-387-48998-8_62.

[24] T. Prešeren, F. Steinman, B. Širok, and T. Bajcar, "The theoretical densimetric froude number values with favourable effect on the clarifier performance," *Chemical Engineering and Processing: Process Intensification*, vol. 74, pp. 97–105, 2013. DOI: https://doi.org/10.1016/j.cep.2013.09.001. [Online]. Available: https://www.sciencedirect.com/science/article/pii/S0255270113001943.

[25] G. I. Barenblatt, "Dimensional analysis and physical similarity," in *Scaling*, ser. Cambridge Texts in Applied Mathematics. Cambridge University Press, 2003, pp. 12–51. DOI: 10.1017/CBO9780511814921.004.

[26] Y. A. Çengal and J. M. Cimbala, *Fluid mechanics: Fundamentals and applications chapter 7 - dimensional analysis and modeling*, Electronic Book, 2010. [Online]. Available: https://www.rose-hulman.edu/Class/me/ES202/Spring%5C%2006-07/Dimensional%5C%20Analysis.pdf.

[27] J. D. Anderson, "Governing equations of fluid dynamics," in *Computational Fluid Dynamics: An Introduction*, J. F. Wendt, Ed. Berlin, Heidelberg: Springer Berlin Heidelberg, 1992, pp. 15–51. DOI: 10.1007/978-3-662-11350-9_2.

[28] J. Pedlosky, "Geophysical fluid dynamics," 1987. DOI: doi.org/10.1121/1.396028.

[29] G. Łukaszewicz and P. Kalita, *Navier–stokes equations - an introduction with applications*, Electronic Book, 2016. DOI: doi.org/10.1007/978-3-319-27760-8.

[30] COMSOL, *Navier-stokes equation*, Web Page, 2015. [Online]. Available: https://www.comsol.com/multiphysics/navier-stokes-equations (visited on 05/15/2021).

[31] H. J. Skadsem, "Meeting regarding modeling.," Personal meeting, 2021.

Appendix A

Rest of results

A.1 Visualization of displacement

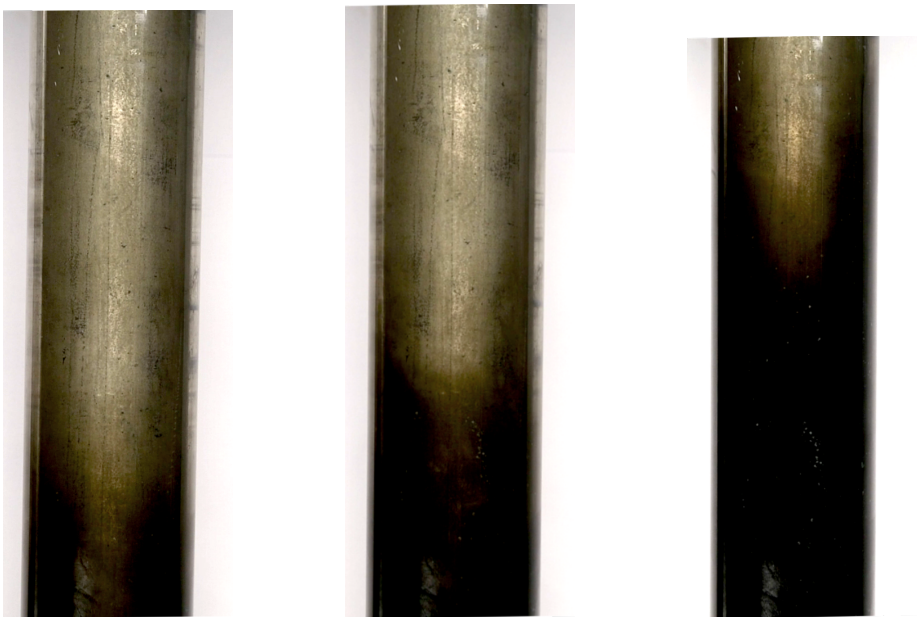

(a) (b) (c)

Figure A.1: *Visualization of displacement: Ecc=0, 2.5Hz*

A.1 Visualization of displacement

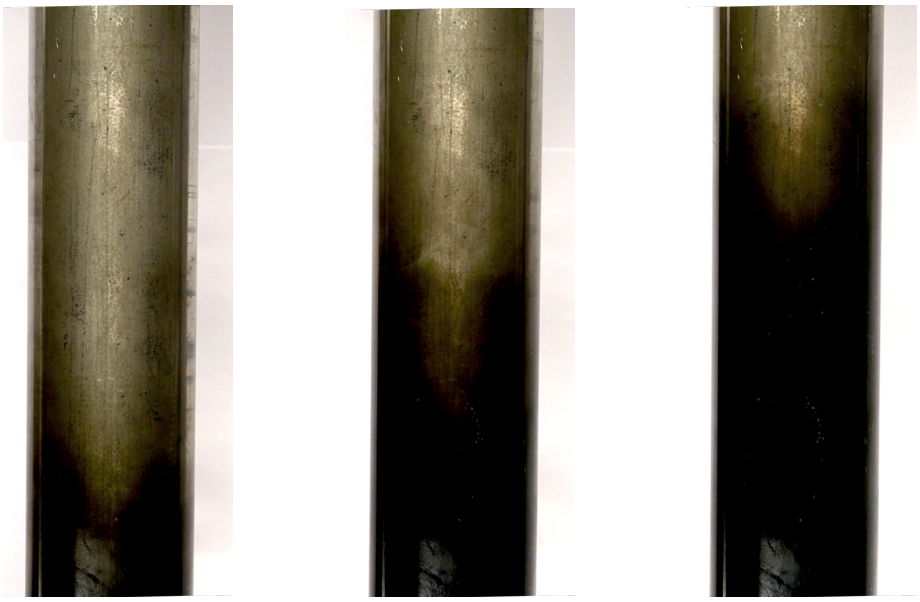

(a) (b) (c)

Figure A.2: *Visualization of displacement: Ecc=0, 5Hz*

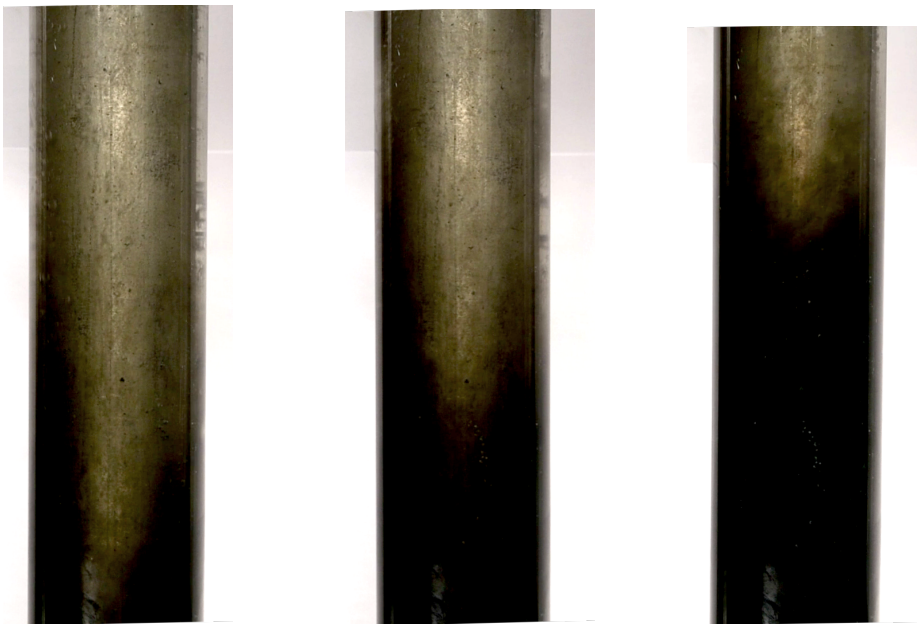

(a) (b) (c)

Figure A.3: *Visualization of displacement: Ecc=0, 10Hz*

A.1 Visualization of displacement

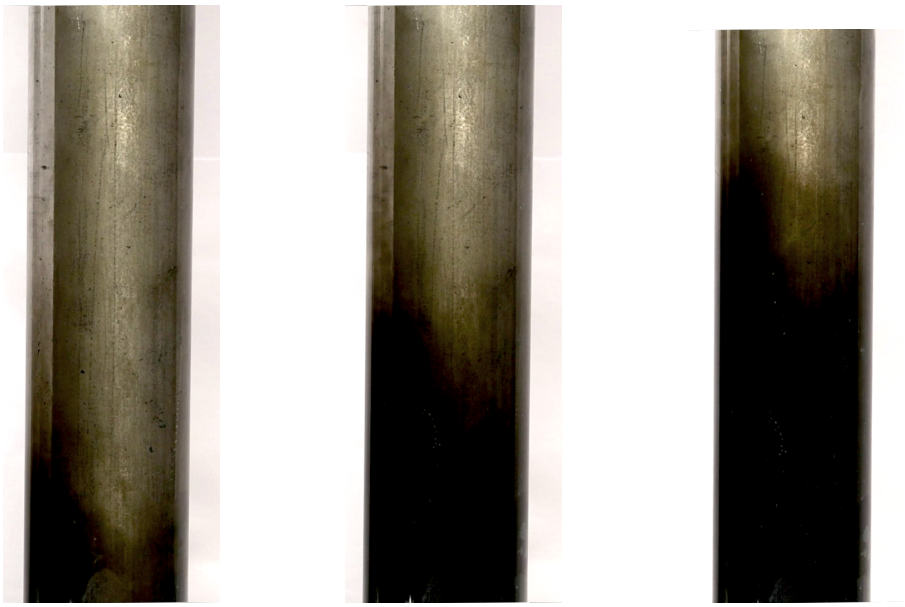

(a) (b) (c)

Figure A.4: *Visualization of displacement: Ecc=0.46, 2.5Hz*

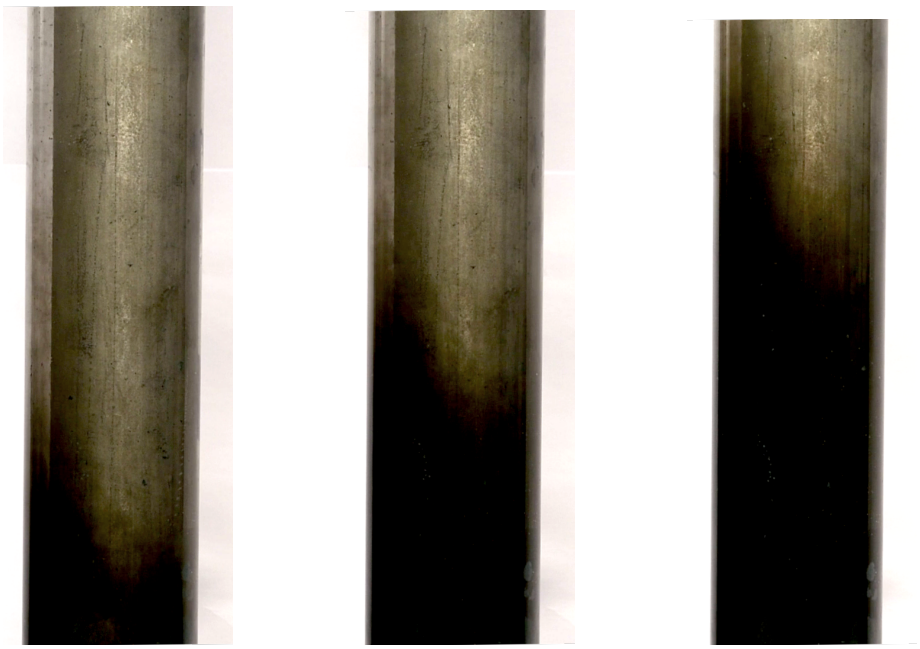

(a) (b) (c)

Figure A.5: *Visualization of displacement: Ecc=0.46, 5Hz*

A.2 Conductivity measurements curves

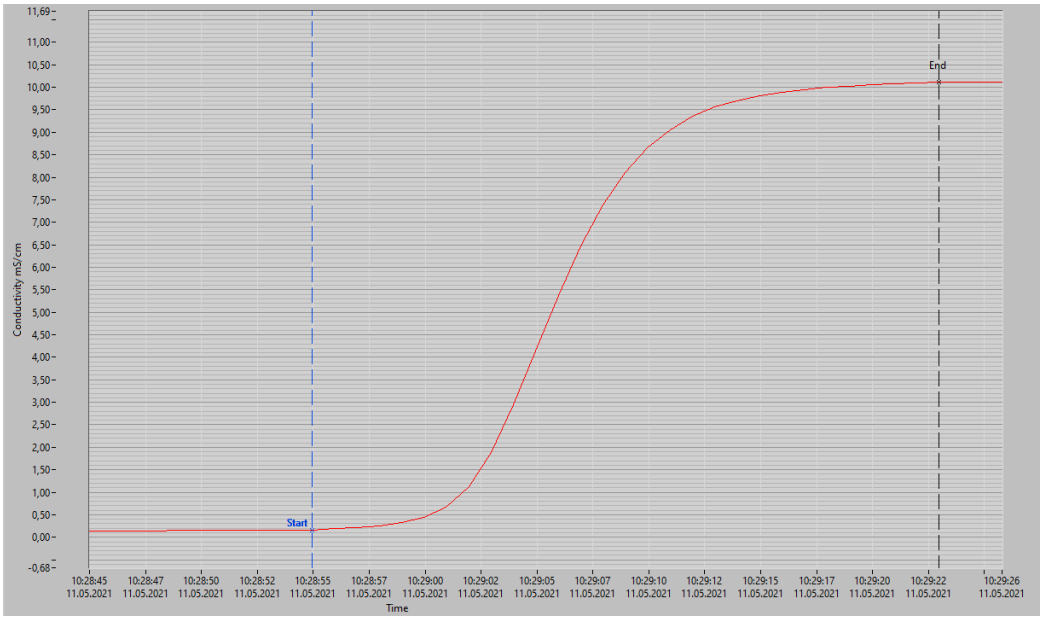

Figure A.6: *Conductivity measurements for Ecc=0, 2.5Hz*

A.2 Conductivity measurements curves

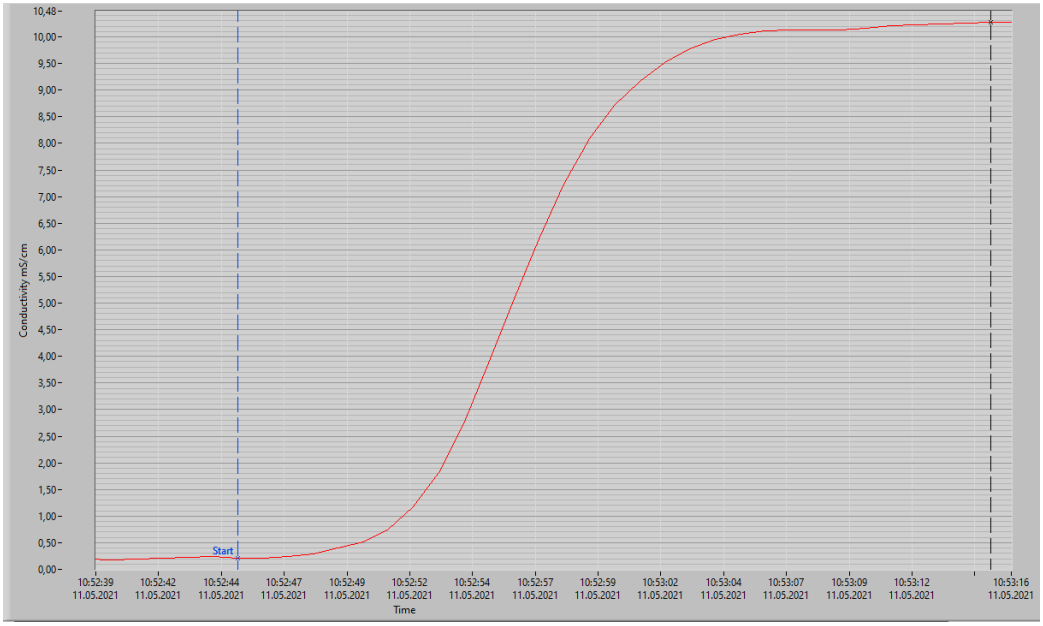

Figure A.7: *Conductivity measurements for Ecc=0, 5Hz*

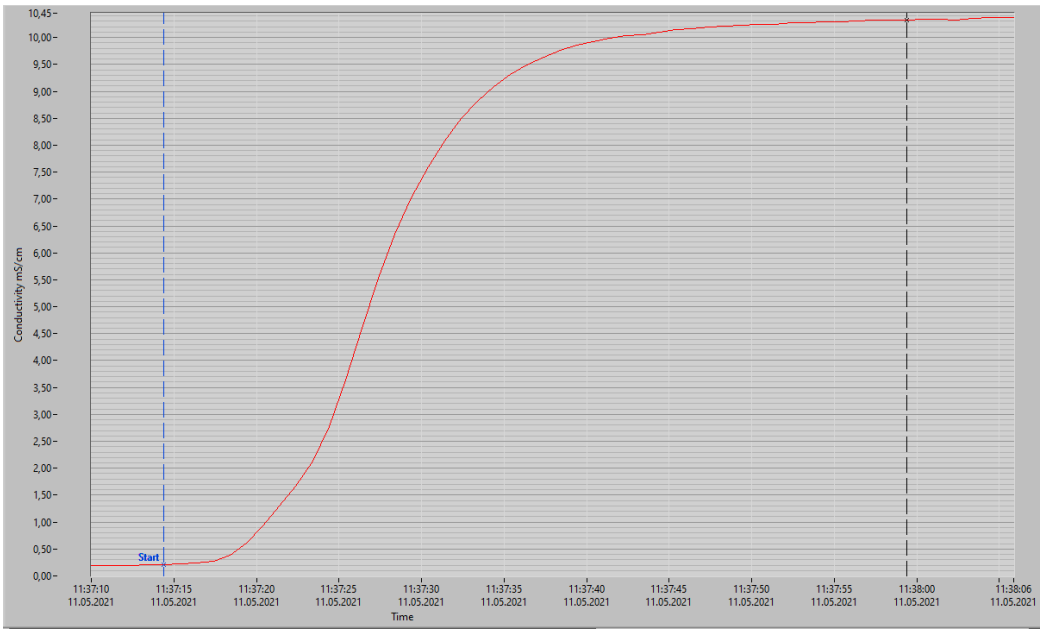

Figure A.8: *Conductivity measurements for Ecc=0, 10Hz*

A.2 Conductivity measurements curves

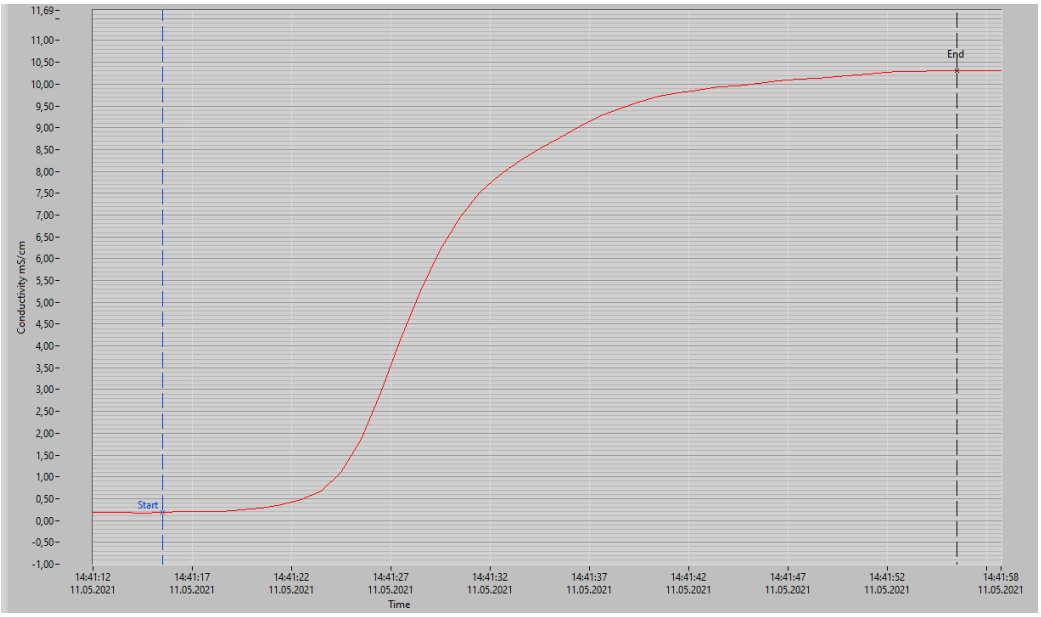

Figure A.9: *Conductivity measurements for Ecc=0.46, 2.5Hz*

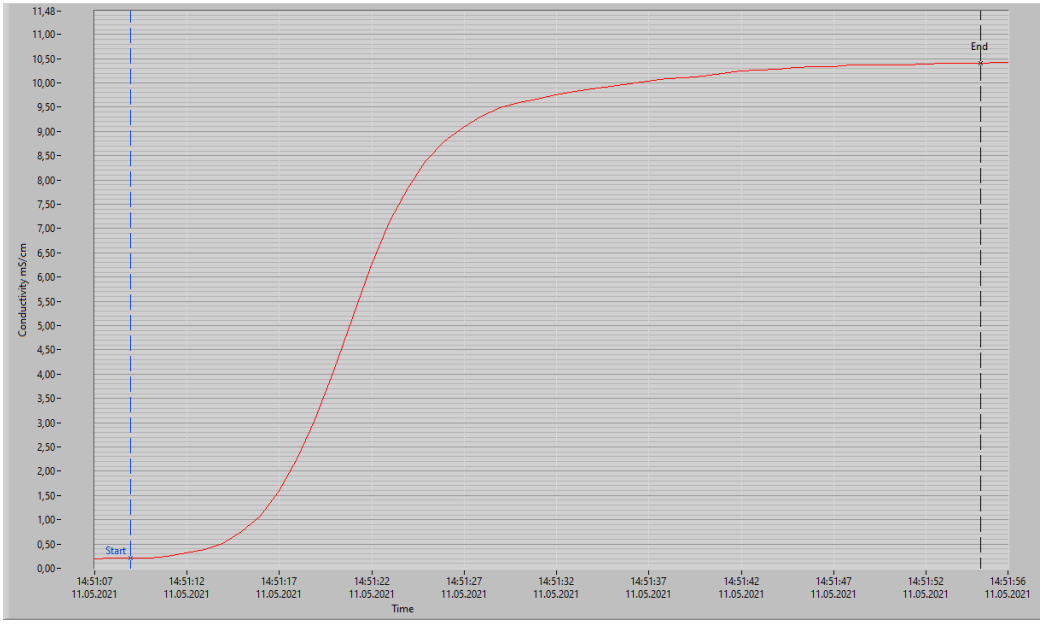

Figure A.10: *Conductivity measurements for Ecc=0.46, 5Hz*

A.2 Conductivity measurements curves

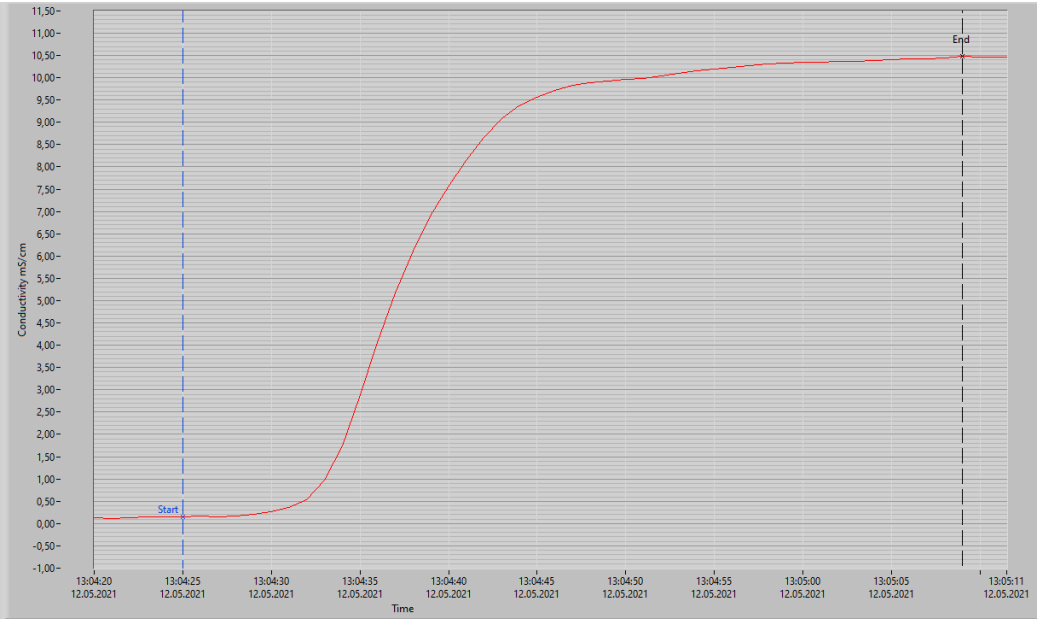

Figure A.11: *Conductivity measurements for Ecc=0.82, 2.5Hz*

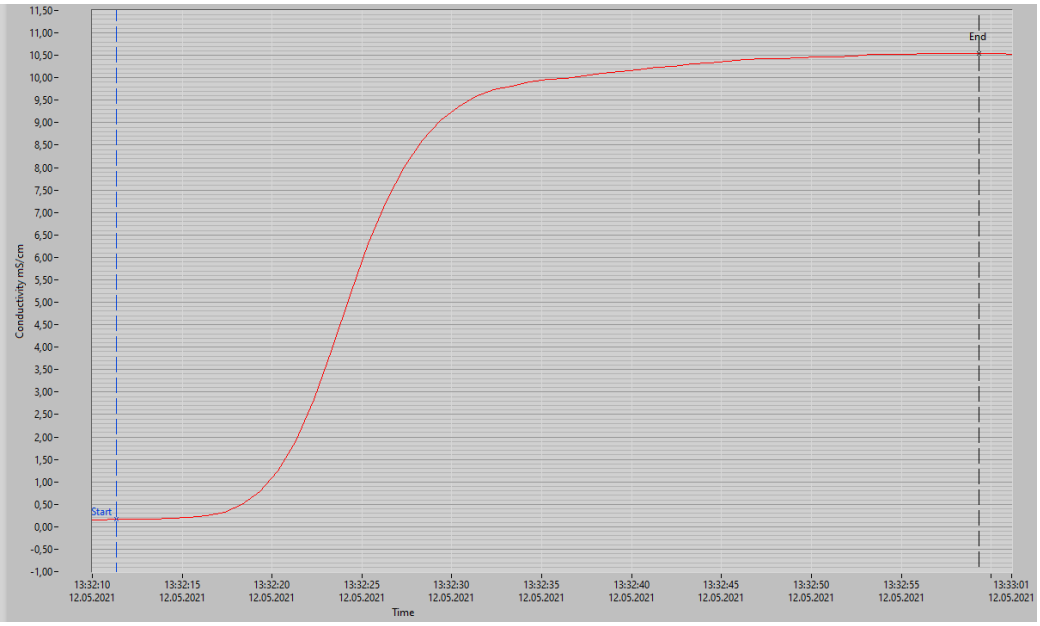

Figure A.12: *Conductivity measurements for Ecc=0.82, 5Hz*

Appendix B

Navier-Stokes

B.1 Rest of the rearrangement of Navier-Stokes with dimensionless numbers

$\overline{\rho}$ is the average density of displacing and displaced fluid:

$$\overline{\rho} = \frac{1}{2}(\rho_1 + \rho_2) \tag{B.1}$$

Furthermore the characteristic velocity scale U_0 such that $\vec{u} = U_0\hat{\vec{u}}$ where $\hat{\vec{u}}$ is an dimensionless velocity vector, and characteristic length scale D_0 such that $x = D_0\hat{x}$ are introduced. The timescale then becomes D_0/U_0 and the Navier stokes equation may be written as:

$$\overline{\rho}(1+\Phi_i At)\frac{U_0^2}{D_0}\left(\frac{\partial\vec{u}}{\partial t} + (\vec{u}\cdot\nabla)\vec{u}\right) = -\frac{p_0}{D_0}\nabla p + \frac{\mu U_0}{D_0^2}\nabla^2 u + \overline{\rho}(1+\Phi_i At)\vec{g} \tag{B.2}$$

where p_0 is a pressure scale. By rearranging equation B.2 we get:

$$(1+\Phi_i At)\underbrace{\frac{\overline{\rho}U_0 D_0}{\mu}}_{=Re}\left(\frac{\partial\vec{u}}{\partial t} + (\vec{u}\cdot\nabla)\vec{u}\right) = -\frac{p_0 D_0}{\mu U_0}\nabla p + \nabla^2 u + (1+\Phi_i At)\frac{\overline{\rho}\vec{g}D_0^2}{\mu U_0} \tag{B.3}$$

Moreover the constant pressure term $\frac{\overline{\rho}\vec{g}D_0^2}{\mu U_0}$ may be absorbed into p:

B.1 Rest of the rearrangement of Navier-Stokes with dimensionless numbers

$$-\frac{p_0 D_0}{\mu U_0}\nabla p + \frac{\overline{\rho}\vec{g}D_0^2}{\mu U_0} \rightarrow -\nabla p' \tag{B.4}$$

where $p_0 = \frac{\mu_0 U_0}{D_0}$ as a pressure scale and let p become $p' + \frac{1}{p_0}\overline{\rho}\vec{g}\cdot\vec{x}$

Now Navier-Stokes becomes:

$$(1+\Phi_i At)Re\left(\frac{\partial\vec{u}}{\partial t} + (\vec{u}\cdot\nabla)\vec{u}\right) = -\nabla p' + \nabla^2\vec{u} + \Phi_i\frac{At\overline{\rho}\vec{g}D_0^2}{\mu U_0} \tag{B.5}$$

The last term in equation B.5 can be written as:

$$\underbrace{\frac{AtgD_0}{U_0^2}}_{=\frac{1}{Fr^2}} \times \underbrace{\frac{\overline{\rho}U_0 D_0}{\mu}}_{=Re} \cdot \underbrace{\vec{e_g}}_{unitvector for gravity} \tag{B.6}$$

Finally the Navier-Stokes equation becomes:

$$(1+\Phi_i At)\,Re\left(\frac{\partial\vec{u}}{\partial t} + \left(\vec{u}\cdot\vec{\nabla}\right)\vec{u}\right) = -\vec{\nabla}p' + \nabla^2\vec{u} + \Phi_i\frac{Re}{Fr^2}\vec{e}_g \tag{B.7}$$

Appendix C

Pictures of some equipment

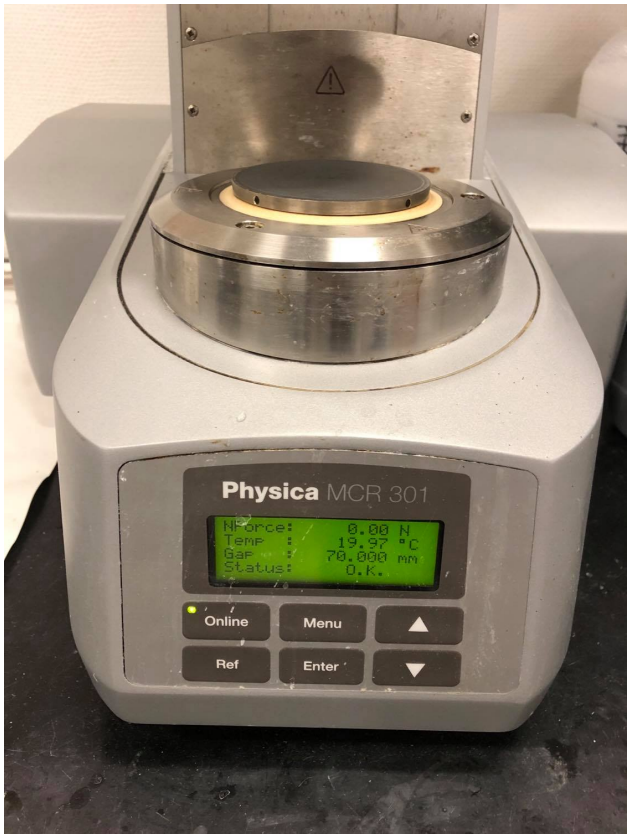

Figure C.1: *Rheometer used, Anton Paar MCR 301*

Figure C.2: *Density meter used, Anton Paar DMA 4500 M*

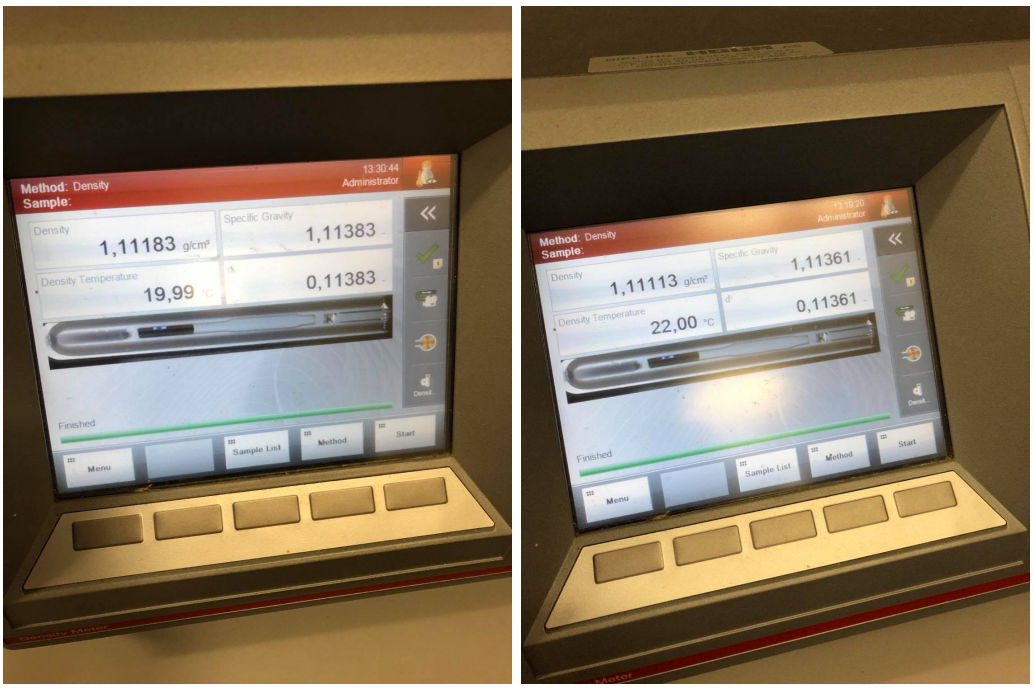

(a) 20 Celsius (b) 22 Celsius

Figure C.3: *Densities of displacing fluid*

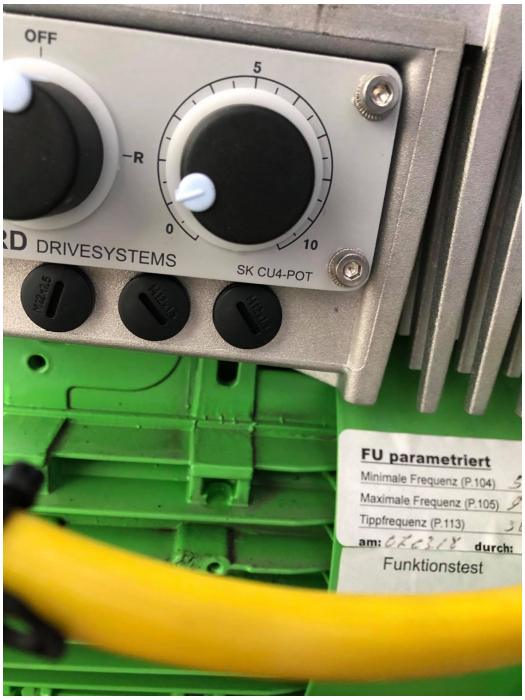

Figure C.4: *The frequency used to obtain 6 L/min*